



Research paper

Isotopic (Sr, Nd, Pb, and Os) composition of highly magnesian dikes of Vestfjella, western Dronning Maud Land, Antarctica: A key to the origins of the Jurassic Karoo large igneous province?

Jussi S. Heinonen^{a,b,*}, Richard W. Carlson^{b,1}, Arto V. Luttinen^{c,2}

^a Department of Geosciences and Geography, University of Helsinki, P.O. Box 64, FI-00014 Helsinki, Finland

^b Department of Terrestrial Magnetism, Carnegie Institution of Washington, 5241 Broad Branch Road, NW Washington, D.C. 20015, USA

^c Finnish Museum of Natural History, University of Helsinki, P.O. Box 17, FI-00014 Helsinki, Finland

ARTICLE INFO

Article history:

Received 9 February 2010

Received in revised form 23 July 2010

Accepted 4 August 2010

Editor: B. Bourdon

Keywords:

Karoo

Continental flood basalt

Petrology

Isotope geochemistry

Ferropicrite

Meimechite

ABSTRACT

There is a substantial debate on the mantle sources and ultimate origins of continental flood basalts (CFBs), e.g., whether they are related to deep-seated thermal upwellings (i.e. mantle plumes) in the upper mantle or not. Here we present high-precision isotopic (Sr, Nd, Pb, and Os) whole-rock data on some primitive dike rocks (ferropicrites, meimechites, picobasalts, and basalts) associated with the Antarctic extension of the Jurassic (~180 Ma) Karoo CFB province. The isotopic data together with previously published trace element data show that the parental melts of the studied rocks sampled two distinctive geochemical reservoirs in the deep sub-Gondwanan mantle. The isotopic signatures of the relatively depleted types show evidence of extensive melt extraction in the past and are indistinguishable from those of mid-ocean ridge basalts (MORBs) of the SW Indian Ridge. On the other hand, the relatively enriched type isotopically resembles modern oceanic island basalts (OIBs) and may sample pyroxenitic sources either formed by melt infiltration in the upper mantle or by reaction of peridotite with recycled oceanic crustal components (with up to 15% of sediment material). The depleted types have previously been associated with anomalously hot mantle sources (> 1600 °C) and mantle plumes, but their MORB-like isotope compositions are unusual for plume-derived rocks. Instead, our findings are more concordant with a recent model [Coltice, N., Bertrand, H., Rey, P., Jourdan, F., Phillips, B.R., Ricard, Y., 2009. Global warming of the mantle beneath continents back to the Archean. *Gondwana Research* 15, 254–266] that suggests the generation of the Karoo CFBs in an extensive melting episode caused by internal heating of the upper mantle beneath the Gondwana supercontinent.

© 2010 Elsevier B.V. All rights reserved.

1. Introduction

Many continental flood basalts (CFBs) show strong lithospheric affinities in their geochemical signatures that make it difficult to deduce the nature of the sublithospheric contribution to these enormous manifestations of mafic magmatism on Earth (e.g., Saunders et al., 1992). This, in part, fuels the ongoing debate on their origin, in particular whether flood basalts are instigated by deep-seated mantle plumes rising to the base of the lithosphere (e.g., Richards et al., 1989) or by “passive” mechanisms like lithospheric delamination (e.g., Elkins-Tanton, 2005), shallow melting anomalies related to extension and distribution of fertile mantle components

(e.g., Anderson, 2007; Foulger, 2007), and internal mantle heating (e.g., Coltice et al., 2007). Some primitive flood basalts may preserve sublithospheric mantle-derived signatures and provide invaluable insight into the deep mantle beneath CFB provinces.

The Jurassic Karoo CFB province represents an outpouring of considerable volumes of basaltic magma (up to 2×10^6 km³; Richards et al., 1989) during the break-up of the Gondwana supercontinent (Fig. 1). The origin of the Karoo CFBs also has been debated: although the great majority of structural analyses, geochemical affinities, and temporal relationships of the majority of Karoo-related rocks point to a strong control of lithosphere on the magmatism (e.g., Hawkesworth et al., 1984; Cox, 1988; Ellam and Cox, 1989; Sweeney et al., 1991, 1994; Luttinen et al., 1998; Elburg and Goldberg, 2000; Luttinen and Furnes, 2000; Jourdan et al., 2004, 2005, 2006, 2007a,b, 2009), the paleostress estimates for the Karoo dikes in Antarctica (Curtis et al., 2008) and high mantle potential temperatures ($T_p > 1500$ – 1600 °C) estimated for the sources of Antarctic ferropicrites and meimechites (Riley et al., 2005; Heinonen and Luttinen, 2008, 2010) are compatible with the plume theory. Recently, warming of the upper mantle by

* Corresponding author. Department of Geosciences and Geography, University of Helsinki, P.O. Box 64, FI-00014 Helsinki, Finland. Tel.: +358 9 191 50802.

E-mail addresses: jussi.s.heinonen@helsinki.fi (J.S. Heinonen), rcarlson@ciw.edu (R.W. Carlson), arto.luttinen@helsinki.fi (A.V. Luttinen).

¹ Tel.: +1 202 478 8474.

² Tel.: +358 9 191 28745.

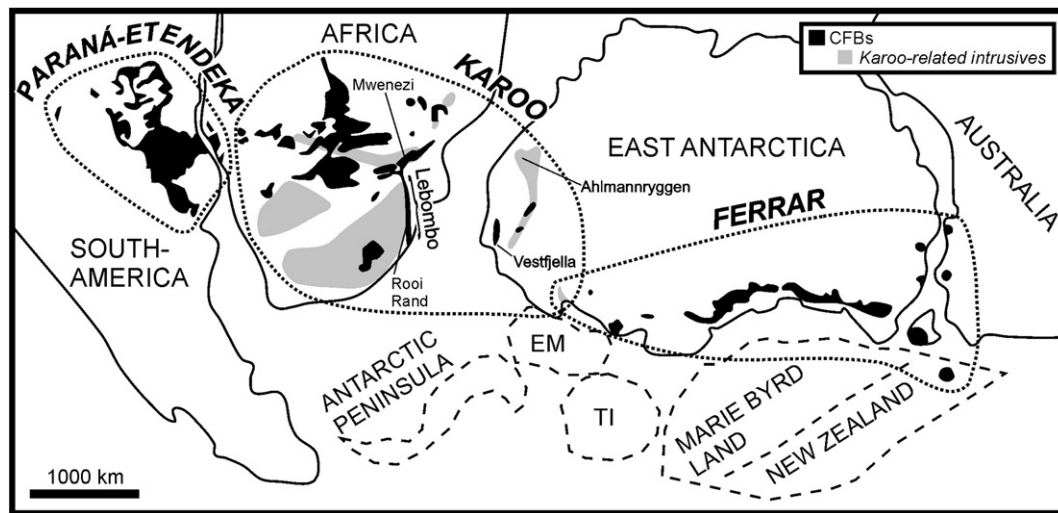


Fig. 1. Distribution of Mesozoic CFBs in reconstructed Gondwana supercontinent. In the case of the Karoo province, the known extent of intrusive equivalents (found outside CFBs) is also shown. EM = Ellsworth-Whitmore Mountains, TI = Thurston Island. Reconstruction modified after Hergt et al. (1991), Storey et al. (1992), Segev (2002), Leat et al. (2006), and Jourdan et al. (2004).

supercontinent-induced insulation and enlargement of the convection wavelength has been suggested as a possible explanation for the generation of the Karoo CFBs (Coltice et al., 2009).

In this study, we present Sr, Nd, Pb, and Os isotopic data on various primitive rock types collected from the Vestfjella mountain range, an Antarctic extension of the Karoo CFB province. In order to probe the isotopic composition and evolution of sublithospheric contributors to Karoo magmatism, we focused on samples (ferropicrites and meimechites) that have previously been considered to derive from the sublithospheric mantle (cf. Heinonen and Luttinen, 2008). These samples include rock types that are both relatively depleted and enriched in incompatible trace elements. Our analysis shows that their isotopic characteristics seem to require two geochemically and lithologically distinct mantle sources. The sources of the depleted and the enriched types can most readily be linked to the depleted upper mantle [source of the mid-ocean ridge basalts (MORBs)] and enriched pyroxenitic mantle components (recycled or melt-metasomatized), respectively. Implications on the origins of the Karoo CFB province and Gondwana break-up processes are discussed.

2. Geological setting and general characteristics of the Vestfjella CFBs and associated rocks

The basal contact of the Vestfjella CFBs is not exposed, but similar to other Karoo-related CFBs of Antarctica (e.g., Harris et al., 1990), they are likely to overlie Paleozoic sedimentary rocks (e.g., Jukes, 1972) that were deposited on Precambrian basement. The basement complex can be divided into two major provinces (Fig. 2): (1) The Grunehogna craton (Wolmarans and Kent, 1982; Krynauw et al., 1991) is thought to consist of an Archean nucleus (Barton et al., 1987) that is almost entirely covered by Mesoproterozoic sedimentary and volcanogenic rocks (Wolmarans and Kent, 1982) and Neoproterozoic mafic intrusions (e.g., Krynauw et al., 1988, 1991; Moyes et al., 1995). (2) The Maud Belt (Groenewald et al., 1995) is characterized by variably metamorphosed supracrustal and intrusive rocks that accreted during the Grenvillian orogeny ~1100 Ma ago and experienced significant tectonic reworking during the Pan-African orogeny ~500 Ma ago (Jacobs et al., 1998, 2003a,b). The Grunehogna craton has been interpreted to represent a fragment of the Zimbabwe-Kaapvaal craton in Africa (e.g., Peters et al., 1991) and the Maud Belt has been thought to be a part of a Natalian-Grenvillian orogenic belt that was formed during the amalgamation of the supercontinent Rodinia (e.g., Jacobs et al., 1993).

The Karoo CFBs were formed in an extensive rift system related to the break-up of the Gondwana supercontinent with the highest volcanic activity occurring ~184–178 Ma ago (Fig. 1; Duncan et al., 1997; Zhang et al., 2003; Jourdan et al., 2005, 2007b; Riley et al., 2005). Other CFB provinces related to the early stages of the southern Gondwana dispersal are the Ferrar province, which is largely contemporaneous with the Karoo event, and the ~130 Ma Paraná-Etendeka CFB province (Fig. 1).

The Karoo-related CFBs of western Dronning Maud Land are exposed in the Vestfjella, Kirwanveggen, and Heimefrontfjella mountain ranges (Fig. 2). Associated dikes are more widespread and are found also from Ahlmannryggen, Mannefallknausane, and H.U. Sverdrupfjella (Figs. 1 and 2; e.g., Harris et al., 1991; Riley et al., 2005; Curtis et al., 2008). Gabbroic intrusions also have been described from the southernmost parts of Vestfjella (Vuori and Luttinen, 2003). At present, the ages of the Karoo-related rocks in western Dronning Maud Land remain relatively poorly constrained, although on the basis of available geochemical, geochronological, and paleomagnetic data, the majority of the volcanic activity can be associated with the main Karoo event in Africa (e.g., Brewer et al., 1996; Duncan et al.,

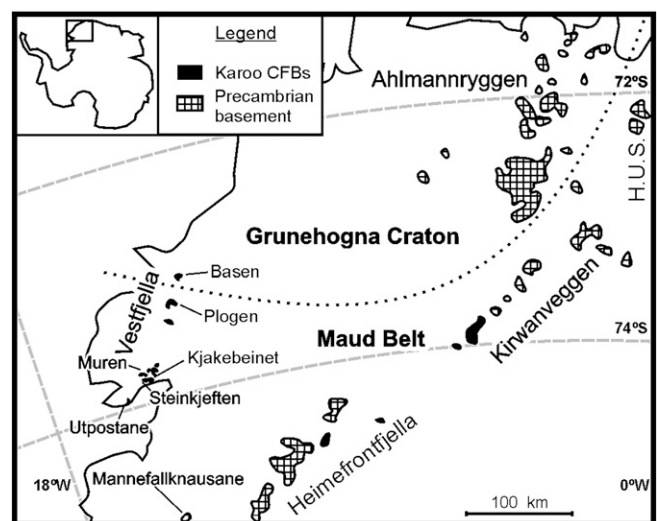


Fig. 2. Distribution of exposed Jurassic continental flood basalts in western Dronning Maud Land, Antarctica. H.U.S. = H. U. Sverdrupfjella. Lithospheric boundary after Corner (1994).

1997; Hargraves et al., 1997; Luttinen and Furnes, 2000; Riley et al., 2005; Zhang et al., 2003).

Although the CFBs of western Dronning Maud Land consist mainly of tholeiites and form a volumetrically minor portion of the Karoo province, they show considerable geochemical heterogeneity in terms of trace element and isotopic compositions (e.g., Furnes et al., 1987; Harris et al., 1990; Luttinen and Siivola, 1997; Luttinen et al., 1998; Luttinen and Furnes, 2000). Luttinen and Siivola (1997) recognized three major lava types at Vestfjella (CT1, CT2, and CT3) that all show strong affinities to continental lithosphere and/or subduction-modified upper mantle (Luttinen and Furnes, 2000). The CFB-associated dikes of western Dronning Maud Land mainly consist of variably contaminated tholeiites and picrites (Harris et al., 1991; Luttinen et al., 1998; Luttinen and Furnes, 2000; Riley et al., 2005), but they also record extreme major element compositions in the form of meimechites (Heinonen and Luttinen, 2010), ferropicrites (Riley et al., 2005; Heinonen and Luttinen, 2008), and ultrapotassic rocks (Luttinen et al., 2002). At Vestfjella, the ferropicrites divide into two distinct compositional types, one showing flat primitive mantle-normalized incompatible element abundances (depleted type) and the other showing more enrichment in the highly incompatible elements (enriched type) (cf. Fig. 3). The former shows notable geochemical similarities with the meimechites that were initially considered as cumulates from ferropicritic or related magmas (Heinonen and Luttinen, 2008). Later mineral chemical analyses revealed, however, that the meimechites were derived from highly magnesian ($\text{MgO} \approx 25 \text{ wt.}\%$) mantle melts generated at high pressures ($\sim 5\text{--}6 \text{ GPa}$), and may closely correspond to the parental melt compositions of the depleted ferropicrites (Heinonen and Luttinen, 2010). The Karoo meimechites and ferropicrites have been linked to high mantle potential temperatures ($>1500\text{--}1600 \text{ }^\circ\text{C}$) compatible with involvement of a mantle plume during the Karoo event (Riley et al., 2005; Heinonen and Luttinen, 2008, 2010). A MORB-like dike (sample P27-AVL) found in Ploggen (Fig. 2) was considered by Luttinen and Furnes (2000) also to represent uncontaminated sublithospheric magma that may correspond to parental melt composition of many Vestfjella lavas.

In comparison with the volumetrically dominant Karoo-related CFBs of southern Africa, the strongly lithosphere-signatured CT1 and CT3 chemical types can be associated with the heterogeneous lavas of the $\sim 184 \text{ Ma}$ Sabie River Basalt Formation (Cox and Bristow, 1984; Duncan et al., 1997) of the southern part of the Lebombo Monocline

(Fig. 1; Luttinen and Furnes, 2000). The parental magmas of the CT2 lavas (and the MORB-like P27-AVL) have been thought to be genetically related to the $\sim 172 \text{ Ma}$ MORB-like Rooi Rand dike swarm (Fig. 1) that is considered to include the only known examples of nearly uncontaminated sublithospheric Karoo magma types in southern Africa (Duncan et al., 1990; Luttinen and Furnes, 2000; Jourdan et al., 2007a, 2007b). Karoo-related ferropicrites and meimechites are only known from Antarctica: the most primitive Karoo rocks found in Africa are the strongly lithosphere-signatured Mwenezi picrites (e.g., Ellam and Cox, 1989, 1991). The adjacent Paraná-Etendeka province, however, includes ferropicrites that are similar to the enriched ferropicrite type of Vestfjella (Fig. 1; Gibson et al., 2000; Heinonen and Luttinen, 2008).

3. Sample selection and characteristics

3.1. Ferropicrites, meimechites, and associated rocks

The main emphasis in the study was given to the highly magnesian ($\text{MgO} = 10\text{--}24 \text{ wt.}\%$) and relatively Fe-rich ($\text{FeO}_{\text{tot}} = 13\text{--}16 \text{ wt.}\%$) rock types (ferropicrites and meimechites) found as dikes at Vestfjella. These include depleted ferropicrites from Basen (sample AL/B16-98) and West-Muren (AL/WM1e-98), depleted meimechites from Basen (AL/B1b-03, AL/B7-03, and AL/B9-03), a depleted picrobasalt from Steinkjeften (117-KHG-91), an enriched ferropicrite from Basen (JSH/B006), and an enriched MgO-rich basalt from Basen (AL/B7-98) (Fig. 2; Table 1).

All samples, apart from equigranular picrobasalt 117-KHG-91, are olivine-porphyrific ($\sim 10\text{--}40 \text{ vol.}\%$ of phenocrysts; $\phi \leq 6 \text{ mm}$). Olivine phenocrysts ($\text{Fo}_{78\text{--}92}$ in cores) are generally in or close to Fe–Mg equilibrium with the host rock (Electronic Appendix A; Heinonen and Luttinen, 2008, 2010) and contain crystallized melt inclusions (ϕ up to 0.8 mm) that consist of varying amounts of Cr-spinel, amphibole, clinopyroxene, and chloritized mesostasis. Clinopyroxene phenocrysts ($\phi \leq 5 \text{ mm}$) are sparse in some samples and the groundmass consists mainly of clinopyroxene, plagioclase, and Fe–Ti oxides; amphibole is also found in the groundmass of the fresh enriched ferropicrite sample (JSH/B006).

Except for JSH/B006, geochemical data for the samples have been reported by Heinonen and Luttinen (2008) (see Table 1). Generalizing, the depleted ferropicrites, meimechites, and associated rocks (hereafter referred to as *D-FP* magma type) have chondrite-normalized ($\text{La}/\text{Sm})_{\text{N}}$ of 1.1–1.4, ($\text{Sm}/\text{Yb})_{\text{N}}$ of 3.2–4.5, and show relative enrichment of V, but show depletion of the most highly-incompatible elements (Fig. 3; Heinonen and Luttinen, 2008). The enriched ferropicrite and basalt (hereafter referred to as *E-FP* magma type) have ($\text{La}/\text{Sm})_{\text{N}}$ of 1.5–1.7, ($\text{Sm}/\text{Yb})_{\text{N}}$ of 4.9–5.5, and show OIB-like incompatible element characteristics (e.g., relatively high Nb and Ta) (Fig. 3; Heinonen and Luttinen, 2008). Sample JSH/B006 represents the recently discovered, relatively fresh middle part of the enriched ferropicrite dike and was thus chosen for the isotopic analyses; previously unpublished geochemical data for this sample are presented in Table 1 (cf. Fig. 3) and representative olivine analyses in Electronic Appendix A. JSH/B006 is compositionally similar to the more altered samples of the same dike in general (AL/B20a-98, 14-KHG-90; Heinonen and Luttinen, 2008), but the large-ion lithophile element (LILE: Rb, Ba, K, and Sr) contents are $\sim 1.3\text{--}1.8$ times higher relative to the altered samples (cf. Heinonen and Luttinen, 2008). This suggests that the altered samples presented by Heinonen and Luttinen (2008) have been subjected to hydrothermal loss of LILEs. The analyzed olivine phenocryst cores in JSH/B006 range from $\text{Fo}_{78\text{--}83}$. Using a $K_d(\text{Fe}\text{--}\text{Mg})^{\text{ol-liq}}$ value of 0.35 (cf. Heinonen and Luttinen, 2008, 2010), Fo_{83} olivine is in Fe–Mg equilibrium with a melt having a Mg# of 60 [$\text{Mg}\# = \text{Mg}/(\text{Mg} + \text{Fe}^{2+})$]. This is lower than the Mg# of JSH/B006 (66) and corresponds more closely to the Mg# of the chilled margin sample AL/B20a-98 (62; Heinonen and Luttinen, 2008)

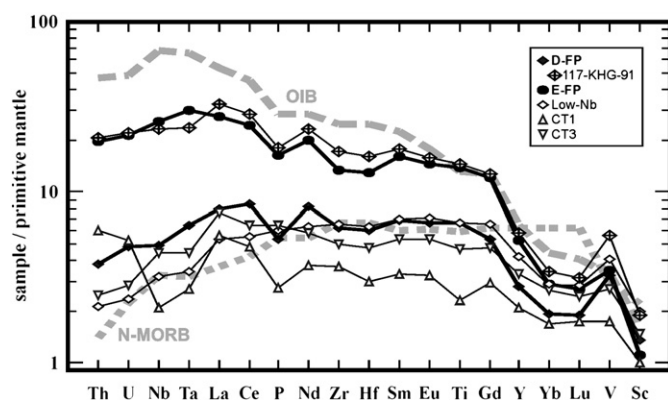


Fig. 3. Primitive mantle-normalized incompatible element patterns of representative D-FP (AL/B9-03 and 117-KHG-91), E-FP (JSH/B006), low-Nb (P4-KHG-90), CT1 (AL/307), and CT3 (sk229-AVL) samples. D-FP sample 117-KHG-91 has high La/Sm and Sm/Yb ratios similar to E-FP, but it exhibits the characteristic low Nb, low Ta, and high V/Lu of D-FP, and has been considered to represent a low-degree melt from D-FP sources (Heinonen and Luttinen, 2008). Average compositions of N-MORB (Sun and McDonough, 1989; V and Sc from Salters and Stracke, 2004) and OIB (Sun and McDonough, 1989; V and Sc calculated after GEOROC: <http://georoc.mpch-mainz.gwdg.de/georoc/>) are shown in gray for comparison. Normalizing values after Sun and McDonough (1989), except for V and Sc, after McDonough and Frey (1989).

Table 1
Whole-rock geochemistry of primitive rock samples from Vestfjella mountain range (western Dronning Maud Land, Antarctica).

Sample	AL/B1b-03*	AL/B7-03*	AL/B9-03*	AL/B16-98*	AL/WM1e-98*	117-KHG-91*	JSH/B006	AL/B7-98*	5-mk-91	P4-KHG-90	AL/307	sk221-AVL	sk229-AVL**
Suite	D-FP	D-FP	D-FP	D-FP	D-FP	D-FP	E-FP	E-FP	Low-Nb	Low-Nb	CT1	CT3	CT3
Rock type	Meimechite	Meimechite	Meimechite	Ferropicrite	Ferropicrite [§]	Picrobasalt	Ferropicrite [§]	Basalt	Olivine cumulate?	Basalt	Olivine cumulate	Olivine cumulate?	Olivine cumulate?
Locality	Basen	Basen	Basen	Basen	Muren	Kjakebeinet	Basen	Basen	Mannefallkn.	Plogen	Plogen	Steinkjeften	Steinkjeften
<i>Major and minor elements [wt.%, normalized to 100% volatile free]</i>													
SiO ₂	46.57	47.05	45.53	45.38	43.65	43.74	44.86	49.07	45.55	49.73	47.50	49.20	48.14
TiO ₂	1.61	1.70	1.44	2.47	2.07	3.31	3.01	3.16	1.31	1.43	0.50	0.98	1.00
Al ₂ O ₃	8.31	8.59	7.01	8.76	8.85	11.63	8.19	11.29	9.09	13.95	7.71	8.80	9.49
FeO _T	13.14	12.87	12.74	14.62	15.10	16.59	16.19	13.69	13.66	10.52	12.42	11.89	13.10
MnO	0.20	0.20	0.19	0.20	0.20	0.21	0.21	0.18	0.19	0.16	0.18	0.19	0.20
MgO	19.21	18.57	24.39	16.71	18.88	11.31	15.54	10.49	19.83	9.09	26.22	16.91	19.13
CaO	9.09	9.24	7.14	9.74	9.02	10.20	9.02	9.37	8.59	12.60	4.64	10.41	7.68
Na ₂ O	1.41	1.41	1.31	1.63	1.53	1.60	1.75	1.76	1.53	2.23	0.66	1.25	1.02
K ₂ O	0.34	0.23	0.15	0.28	0.50	1.00	0.87	0.59	0.14	0.16	0.13	0.28	0.10
P ₂ O ₅	0.12	0.13	0.12	0.21	0.19	0.41	0.36	0.39	0.11	0.13	0.06	0.10	0.14
LOI	1.55	1.23	1.04	1.07	1.58	1.67	2.42	3.86	–	–	–	–	4.00
Mg# [†]	74	74	79	69	71	57	66	60	74	63	81	74	74
<i>Trace elements [ppm]</i>													
Cr (XRF)	1211	1132	1252	931	1022	410	579	357	1175	640	1195	2115	1413
Ni	848	807	1270	732	880	375	660	370	943	226	1321	516	642
V	306	321	265	401	364	487	285	258	290	334	144	293	223
Zr	77	80	69	131	104	202	151	160	66	73	41	56	56
Ba (ICP-MS)	106	56	25	51	91	393	225	165	30	50	60	147	71
Rb	9.2	6.7	3.6	6.8	8.4	20.0	20.8	7.9	7.0	3.8	10.5	5.5	3.0
Sr	251	242	188	321	303	768	520	404	156	227	76	173	125
Ta	0.39	0.41	0.26	0.62	0.43	1.00	1.24	1.23	0.20	0.14	0.11	0.15	0.18
Nb	5.22	5.55	3.46	9.10	6.05	17.22	18.54	17.06	2.75	2.28	1.50	2.55	3.13
Sc	26	28	23	30	28	36	19	21	28	34	17	33	25
Hf	2.10	2.19	1.85	3.53	2.74	5.18	4.04	4.10	1.86	1.95	0.92	1.36	1.46
Y	14.05	15.10	12.81	20.05	16.65	27.85	23.74	28.22	16.52	19.04	9.54	13.69	15
Th	0.43	0.45	0.32	0.86	0.49	1.83	1.69	1.86	0.32	0.18	0.51	0.21	0.21
U	0.13	0.14	0.10	0.21	0.15	0.48	0.45	0.46	0.09	0.05	0.11	0.06	0.06
La	7.06	7.53	5.48	11.38	7.75	23.27	18.94	17.88	4.03	3.63	3.82	4.21	5.19
Ce	18.74	20.05	15.09	29.12	19.78	52.28	43.71	38.20	10.11	9.76	8.53	10.19	11.40
Nd	12.91	13.83	11.15	19.91	14.51	32.61	27.39	23.49	8.33	8.53	5.08	7.40	7.77
Sm	3.42	3.64	3.05	5.43	4.32	8.26	7.12	7.10	2.78	3.08	1.48	2.22	2.35
Eu	1.19	1.28	1.11	1.89	1.52	2.77	2.47	2.61	1.04	1.18	0.55	0.83	0.89
Gd	3.54	3.73	3.17	5.42	4.46	7.95	7.21	7.55	3.37	3.87	1.76	2.70	2.80
Tb	0.55	0.59	0.51	0.82	0.68	1.17	1.10	1.18	0.59	0.64	0.31	0.46	0.48
Yb	1.08	1.15	0.95	1.30	1.06	1.81	1.42	1.59	1.18	1.40	0.83	1.14	1.30
Lu	0.16	0.16	0.14	0.18	0.15	0.25	0.20	0.22	0.17	0.21	0.13	0.18	0.18

Analyses performed at the Geoanalytical Lab of the Washington State University; see Heinonen and Luttinen (2008) for analytical methods. Totals of major element oxides range 98–100 wt.%. For trace elements from Cr to Zr XRF-values given and for trace elements from Ba to Lu ICP-MS values given.

* Data from Heinonen and Luttinen (2008).

** Data from Luttinen and Furnes (2000); § = represents cumulate parts of a ferropicritic dike. † = Mg-number [atomic Mg/(Mg + Fe²⁺); Fe²⁺/Fe_{tot} = 0.9].

indicating that JSH/B006 represents cumulate parts of the enriched ferropicrite dike.

3.2. Other samples

Five samples from other primitive olivine-phyric dikes and lava flows of Vestfjella were analyzed as a reference dataset. Lava sample sk229-AVL represents the CT3 magma type and its major and trace element data have been reported by Luttinen and Furnes (2000). Previously unpublished geochemical data for the samples AL/307, sk221-AVL, P4-KHG-90, and 5-mk-91 are presented in Table 1. Sample AL/307 represents cumulate parts of a lava flow at Plogen (Fig. 2) and, on the basis of its low Ti/P (~10) and Ti/Zr (~70), can be grouped as CT1 (cf. Luttinen and Furnes, 2000). Sample sk221-AVL has been collected from an olivine-phyric lava flow at Steinkjeften (Fig. 2). It shows geochemical affinity to CT3 by having low Ti/P (~13) but high Ti/Zr (~110) (cf. Luttinen and Furnes, 2000). Samples P4-KHG-90 and 5-mk-91 represent two dikes from Plogen and Mannefallknasane, respectively (Fig. 2). The latter is found crosscutting a Precambrian granite. On the basis of their high Ti/P (15–16), high Ti/Zr (~120), low Nb/Y and low (La/Sm)_N (0.7–0.9) they can be associated with the MORB-like dike found at Plogen (P27-AVL; cf. Luttinen and Furnes, 2000). These three samples (P4-KHG-90, 5-mk-91, and P27-AVL) are hereafter referred to as *low-Nb* magma type.

4. Analytical methods

For the analytical information concerning the XRF (ThermoARL Advant'XP+) and ICP-MS (HP 4500+) methods at the GeoAnalytical Lab of the Washington State University, the reader is referred to Heinonen and Luttinen (2008), where detailed descriptions of precision and accuracy and data on international standard sample are provided (see also Johnson et al., 1999; Knaack et al., 1994).

The majority of the isotopic analyses (Sr, Nd, Pb, and Os) were performed at the Department of Terrestrial Magnetism (DTM), Carnegie Institution of Washington. Prior to analyses, the hand-sized samples were covered with a cloth and crushed to smaller pieces with a rock hammer. The freshest pieces were carefully hand-picked, crushed in a ceramic jaw crusher, and powdered in a ceramic mill in order to avoid contamination with Re, Os, and Pb. Between each run the crushing devices were purified with aliquots of clean quartz.

Approximately 50–100 mg of sample powder was separated for the Sr, Nd, and Pb analyses. The powders were dissolved in a 4:3 mixture of concentrated HF and HNO₃ at 150 °C (2 h in a CEM microwave oven). Prior to dissolution, the samples were spiked with enriched tracers of ⁸⁷Rb, ⁸⁴Sr, ¹⁵⁰Nd, ¹⁴⁹Sm, ²⁰⁵Pb, and ²³⁵U. This was followed by drying and treatments with concentrated HNO₃ (twice, evaporation in between) and 12 N HCl. The dried samples were then treated twice with 0.5 N HBr (evaporation in between) and loaded into 0.04 ml columns containing cleaned AG1-X8 anion-exchange resin. Rb, Sr, Sm, Nd, and U were eluted together with matrix elements in 0.5 N HBr whereas Pb stuck to the resin and was subsequently eluted in 0.5 N HNO₃. The Pb splits were then dried, dissolved in 0.5 N HBr, and passed through the columns again to purify the split.

The 0.5 N HBr matrix solutions containing Rb, Sr, Sm, Nd, and U were dried, treated with water and concentrated HNO₃, and dried again. The samples were then treated with 4 N HCl, dried, and dissolved in 1.25 N HCl to be loaded into primary columns (0.6*20 cm) containing cleaned AG50W-X8 cation-exchange resin. Rb and U were eluted between 14–24 ml and Sr between 32–46 ml with 2.5 N HCl. REE were eluted with 4 N HCl between 12–28 ml. All splits were then dried under heat lamp.

The splits containing Rb and U were dissolved in 1.5 ml of 2 N HNO₃ and loaded in 0.25 ml columns containing cleaned TRU resin. Rb was collected from the loading volume and from additional wash with 4 ml of 2 N HNO₃. U stuck to the resin and was subsequently eluted with

4 ml of 0.1 N HCl–0.3 N HF. The REE splits were dissolved in 0.04 ml of 0.1 N HCl and loaded in 0.2*20 cm columns containing AG50-X8 cation-exchange resin in NH₄⁺ form. Sm and Nd were separated from each other and from other REE using α-hydroxyisobutyric acid as an eluent.

Re–Os extractions were made from separate 1000–2000 mg cuts of sample powder. The powders were poured into Carius tubes along with spike solutions containing enriched tracers of ¹⁸⁵Re and ¹⁹⁰Os. Prior to addition of 8 ml of aqua regia, the tubes were chilled by immersing them in a solid CO₂-methanol slush. Tubes were then welded shut and placed into an oven at 240 °C overnight. After cooling, the tubes were frozen, depressurized, cut open, and the solutions were poured into 50 ml test tubes. Os was extracted from the solution into 9 ml of CCl₄ (in three 3 ml steps) leaving aqua regia (now containing Re) and insoluble rock sludge behind. Os was back extracted from the CCl₄ solution into 4 ml of concentrated HBr and dried under heat lamp. The Os samples were then dissolved in a CrO₃–12 N H₂SO₄ mixture and microdistilled using the technique described by Roy-Barman and Allègre (1994). The Re-bearing solutions were dried, dissolved in 10 ml of 1 N HCl, and loaded into cleaned 0.6*4 cm columns containing AG-1 X8 anion-exchange resin. Re stuck to the resin that was washed with 10 ml of 1 N HCl, 2.5 ml of 0.8 N HNO₃, and 2 ml of 4 N HNO₃ to remove other elements. Re was then eluted in 10 ml of 4 N HNO₃, dried, and dissolved in 1 ml of 0.1 N HNO₃. The Re samples were further purified by loading them into cleaned and equilibrated 0.25 ml columns containing AG-1 X8 anion-exchange resin. Columns were washed with 8 ml of 0.1 N HNO₃ and Re was eluted in 5 ml of 8 N HNO₃. Finally, after drying, 0.05 ml of H₂O₂ was added to the Re samples and they were once again evaporated to dryness.

Isotopic compositions of Rb, Sm, U, and Re for isotope-dilution concentration determinations (Table 2) were measured on the DTM VG-P54 multiple-collector ICP-MS. Rb and Sm were measured statically using Faraday cups whereas the majority of U measurements and all Re measurements were obtained on the Daly detector system. During the Sm measurements Nd and Gd interferences were monitored and mass fractionation was internally corrected to ¹⁴⁷Sm/¹⁵²Sm = 0.56081. Instrument fractionation for Rb, U, and Re was estimated by normalizing to bracketing standard runs. Analytical precisions for concentrations are estimated as follows: Rb = 1%, Sm = 0.1%, U = 2%, and Re = 2%.

Isotopic compositions of Pb (Table 2) were also measured on the DTM VG-P54. All samples contained enough Pb to measure statically using Faraday cups. Mass fractionation for Pb was controlled by comparing bracketing runs of NBS-981 standard to values reported by Todt et al. (1996). The standard runs yielded the following average ratios: ²⁰⁶Pb/²⁰⁴Pb = 17.289 ± 0.009 (2σ), ²⁰⁷Pb/²⁰⁴Pb = 15.979 ± 0.009, and ²⁰⁸Pb/²⁰⁴Pb = 38.250 ± 0.028 (n = 5).

Isotopic compositions of Sr, Nd, and Os (Table 2) were determined by thermal ionization mass spectrometry (TIMS) using the DTM Thermo-Fisher Triton. The Sr samples were analyzed statically using single Re filaments, monitoring all Sr isotopes and ⁸⁵Rb, and correcting for fractionation to ⁸⁶Sr/⁸⁸Sr = 0.1194. Sr isotopic data in Table 2 are reported relative to the NBS-987 standard (⁸⁷Sr/⁸⁶Sr = 0.71025) that gave an average ⁸⁷Sr/⁸⁶Sr of 0.710242 ± 0.000007 (2σ) in three intervening runs. The Nd samples were measured statically using double Re filaments to produce a Nd+ ion beam, monitoring interferences from Ce and Sm, and correcting for fractionation to ¹⁴⁶Nd/¹⁴⁴Nd = 0.7219. Nd isotopic data in Table 2 are reported relative to the JNdi standard (¹⁴³Nd/¹⁴⁴Nd = 0.512100) that gave an average ¹⁴³Nd/¹⁴⁴Nd of 0.512105 ± 0.000003 (2σ) in four intervening runs. The Os measurements were obtained on the single electron multiplier by running Os as the OsO₃⁻ ion on Pt filaments covered with Ba(OH)₂, monitoring interferences from Re, and correcting for fractionation to ¹⁹²Os/¹⁸⁸Os = 3.082614. Five intervening runs of the internal DTM Johnson Matthey Os standard yielded an average ¹⁸⁷Os/

Table 2
Whole-rock Sr, Nd, Pb, and Os isotopic composition of primitive rock samples from Vestfjella (western Dronning Maud Land, Antarctica).

Sample	AL/B1b-03	AL/B7-03	AL/B9-03 [®]	AL/B16-98 [†]	AL/WM1e-98 [†]	117-KHG-91	JSH/B006	AL/B7-98 [†]	5-mk-91	P4-KHG-90	AL/307	sk221-AVL	sk229-AVL
Suite	D-FP	D-FP	D-FP	D-FP	D-FP	D-FP	E-FP	E-FP	Low-Nb	Low-Nb	CT1	CT3	CT3
Rb [ppm]	7.47	6.15	4.45	6.84	8.37	16.72	20.32	7.85	7.47	4.14	9.53	5.16	2.51
Sr [ppm]	240	263	220	321	303	455	516	415	161	234	66	151	119
⁸⁷ Rb/ ⁸⁶ Sr	0.09010	0.06763	0.05860	0.06165	0.07992	0.10634	0.11394	0.05472	0.13427	0.05123	0.41641	0.09847	0.06101
⁸⁷ Sr/ ⁸⁶ Sr (m)	0.703833 ± 09	0.703302 ± 08	0.703112 ± 07 [§]	0.703118 ± 20	0.703200 ± 50	0.703844 ± 08	0.704572 ± 07 [§]	0.705180 ± 50	0.703692 ± 30	0.703348 ± 20	0.708039 ± 07 [§]	0.704810 ± 09	0.705088 ± 07
(⁸⁷ Sr/ ⁸⁶ Sr) _{180 Ma}	0.703602	0.703129	0.702962	0.702960	0.702995	0.703572	0.704280	0.705040	0.703348	0.703217	0.706973	0.704558	0.704932
Sm [ppm]	3.23	3.79	3.24	6.11	5.10	7.39	6.65	7.28	2.70	2.99	1.26	1.80	1.84
Nd [ppm]	13.16	15.48	12.54	23.51	18.89	32.47	27.10	27.27	8.83	9.40	4.57	6.36	6.85
¹⁴⁷ Sm/ ¹⁴⁴ Nd	0.1484	0.1482	0.1564	0.1572	0.1633	0.1377	0.1483	0.1615	0.1849	0.1923	0.1668	0.1710	0.1623
¹⁴³ Nd/ ¹⁴⁴ Nd (m)	0.513006 ± 03	0.513004 ± 03	0.512985 ± 03	0.512958 ± 10	0.513008 ± 10	0.512829 ± 04	0.512757 ± 04	0.512688 ± 12	0.513014 ± 10	0.513000 ± 13	0.512055 ± 04	0.512589 ± 04	0.512523 ± 04
(¹⁴³ Nd/ ¹⁴⁴ Nd) _{180 Ma}	0.512831	0.512829	0.512801	0.512773	0.512816	0.512667	0.512582	0.512498	0.512796	0.512773	0.511858	0.512388	0.512332
(ε _{Nd}) _{180 Ma} [#]	8.3	8.3	7.7	7.2	8.0	5.1	3.5	1.8	7.6	7.2	−10.7	−0.9	−2.2
Re [ppb]	0.530	0.737	0.537 (0.534)	0.671	0.795	0.490	0.548	0.440	0.361	0.787	0.067	0.173	0.228
Os [ppb]	2.880	1.222	2.646 (2.358)	1.407	0.898	−0	0.154	0.257	1.836	0.543	3.024	2.395	2.019
¹⁸⁷ Re/ ¹⁸⁸ Os	0.887	2.910	0.978 (1.091)	2.300	4.271	−	17.290	8.299	0.948	7.003	0.106	0.349	0.545
¹⁸⁷ Os/ ¹⁸⁸ Os (m) [§]	0.12857	0.13435	0.12862 (0.12893)	0.13317	0.14050	−	0.19200	0.16747	0.12921	0.14965	0.13070	0.13189	0.13138
(¹⁸⁷ Os/ ¹⁸⁸ Os) _{180 Ma}	0.12590	0.12561	0.12568 (0.12565)	0.12626	0.12768	−	0.14008	0.14255	0.12636	0.12862	0.13038	0.13085	0.12974
U [ppm] [*]	0.14	0.18	0.13	0.21	0.15	0.47	0.45	0.46	0.09	0.05	0.08	0.05	0.06
Th [ppm] [*]	0.43	0.45	0.32	0.86	0.49	1.83	1.69	1.86	0.32	0.18	0.51	0.21	0.21
Pb [ppm]	0.84	1.03	0.93	1.79	1.27	2.34	2.27	2.08	1.07	0.65	0.72	0.91	1.24
²³⁸ U/ ²⁰⁴ Pb	10.3	10.7	8.5	7.3	7.3	12.4	12.3	13.8	5.3	4.8	6.7	3.5	3.1
²³² Th/ ²⁰⁴ Pb	33.0	28.1	22.3	31.0	24.8	50.2	48.5	58.3	19.5	17.8	23.1	12.0	10.7
²⁰⁶ Pb/ ²⁰⁴ Pb (m) [§]	18.111	18.122	17.961	18.103	17.825	17.701	18.256	18.260	18.351	17.809	17.203	17.380	17.374
²⁰⁷ Pb/ ²⁰⁴ Pb (m) [§]	15.491	15.504	15.473	15.489	15.492	15.437	15.543	15.598	15.597	15.523	15.440	15.535	15.541
²⁰⁸ Pb/ ²⁰⁴ Pb (m) [§]	37.74	37.73	37.69	37.78	37.52	37.79	38.26	38.28	38.31	37.57	37.93	37.17	37.16
(²⁰⁶ Pb/ ²⁰⁴ Pb) _{180 Ma}	17.820	17.818	17.721	17.896	17.619	17.349	17.908	17.868	18.201	17.674	17.012	17.280	17.285
(²⁰⁷ Pb/ ²⁰⁴ Pb) _{180 Ma}	15.477	15.489	15.461	15.479	15.482	15.420	15.525	15.579	15.589	15.516	15.430	15.530	15.537
(²⁰⁸ Pb/ ²⁰⁴ Pb) _{180 Ma}	37.44	37.48	37.49	37.50	37.30	37.34	37.82	37.76	38.13	37.41	37.53	37.04	37.06

Within-run error expressed as 2σ_m in the last significant digits for the measured ratios (m), except for the ones marked with [§] external error assigned (see Section 4).

[®] Os data for duplicate sample powder given in parentheses.

[#] Calculated using ¹⁴³Nd/¹⁴⁴Nd = 0.512636 and ¹⁴⁷Sm/¹⁴⁴Nd = 0.1966.

[†] Sr and Nd isotopic data from Heinonen and Luttinen (2008).

^{*} U and Th concentrations printed in italics have been analyzed with ICP-MS at the Washington State University GeoAnalytical Laboratory (cf. Table 1).

^{188}Os of 0.17324 ± 0.00016 (2σ). Sample 117-KHG-91 did not contain enough Os for proper isotopic determinations.

In the Pb and Os measurements, the external errors were larger than in-run precisions and thus the uncertainty for these elements are assigned to the former in Table 2. During the Sr and Nd runs, the external errors were usually slightly smaller than the in-run precisions (cf. Table 2). The aforementioned extraction techniques and mass spectrometry resulted in total blanks that posed negligible corrections for element concentrations and isotopic ratios in all samples. Duplicate Re–Os isotopic analysis on sample AL/B9-03 indicates reproducibilities for Re, Os, and $^{187}\text{Os}/^{188}\text{Os}$ results of 0.6%, 11%, and 0.2%, respectively.

Sr and Nd isotopic determinations for samples AL/B16-98, AL/WM1e-98, AL/B7-98, P4-KHG-90, and 5-mk-91 have been performed at the Geological Survey of Finland (GSF). The original datasets for the former three samples have been reported by Heinonen and Luttinen (2008) and the data for the latter two are previously unpublished. All of these samples have been analyzed during the same session and reader is referred to Heinonen and Luttinen (2008) for the descriptions of the analytical procedures at GSF. The comparability of the Sr and Nd analyses performed at GSF and DTM is relatively good on the basis of individual analyses on the different samples of the enriched ferropicritic dike that resulted in isotopic compositions of initial $^{87}\text{Sr}/^{86}\text{Sr} = 0.704320\text{--}0.70434$ and $^{143}\text{Nd}/^{144}\text{Nd} = 0.512564\text{--}0.512591$ at GSF (samples 14-KHG-90 and AL/B20a-98; Luttinen et al., 1998; Heinonen and Luttinen, 2008), and initial $^{87}\text{Sr}/^{86}\text{Sr} = 0.704280$ and $^{143}\text{Nd}/^{144}\text{Nd} = 0.512582$ at DTM (sample JSH/B006; Table 2; Fig. 4) at 180 Ma.

5. Results

Sr, Nd, Pb, and Os isotopic data of the analyzed samples are shown in Table 2 and illustrated in Figs. 4–6. Initial isotopic ratios and ϵ_{Nd} values of the Vestfjella data have been calculated at 180 Ma.

5.1. Ferropicrites, meimechites, and associated rocks

The D-FP compositional type exhibits very unradiogenic initial $^{87}\text{Sr}/^{86}\text{Sr}$ (0.7030–0.7036) and radiogenic initial ϵ_{Nd} (from +5.1 to +8.3) in

general whereas E-FP exhibit more radiogenic initial $^{87}\text{Sr}/^{86}\text{Sr}$ (0.7043–0.7050) and unradiogenic initial ϵ_{Nd} (from +1.8 to +3.5) (Table 2; Fig. 4). The initial Sr and Nd compositions fall within or very close to the ranges of the previously reported values for the respective geochemical types (Fig. 4).

In Pb–Pb space, D-FP and E-FP exhibit moderately unradiogenic initial $^{206}\text{Pb}/^{204}\text{Pb}$ values ranging 17.35–17.90 and 17.87–17.91, respectively (Table 2; Fig. 5). The initial $^{207}\text{Pb}/^{204}\text{Pb}$ and $^{208}\text{Pb}/^{204}\text{Pb}$ ratios of E-FP (15.53–15.58 and 37.76–37.82, respectively) are higher than those of D-FP (15.42–15.49 and 37.30–37.50, respectively) (Table 2).

The Os contents of D-FP are relatively high (0.9–2.9 ppb) and comparable to concentrations reported for komatiites (cf. Shirey and Walker, 1998) apart from microbasaltic sample 117-KHG-91 that did not contain sufficient Os for proper isotopic analysis (Table 2). The Os contents of E-FP are lower (0.2–0.3 ppb) and comparable to those of OIBs (Table 2; cf. Shirey and Walker, 1998). Re contents of the samples range from 0.44 to 0.79 ppb (Table 2). In terms of Os isotopic composition, E-FP shows distinctly more radiogenic initial $^{187}\text{Os}/^{188}\text{Os}$ ratios (0.1401–0.1425) relative to D-FP (0.1256–0.1277) (Table 2; Fig. 6).

In a global comparison, the initial isotope composition of D-FP shows highly radiogenic Nd and relatively unradiogenic Sr, Pb, and Os similar or close to DM and MORB from the SW Indian Ridge (Figs. 4–6) that is the modern successor of the Jurassic Africa–Antarctica rift (cf. Fig. 1). The Group 3 dikes from Ahlmannryggen are the only Karoo magma type that shows equally radiogenic ϵ_{Nd} (5.0–9.0), but they also exhibit more radiogenic $^{87}\text{Sr}/^{86}\text{Sr}$ (0.7035–0.7062; Fig. 4a; cf. Riley et al., 2005) at 180 Ma. Anomalous D-FP sample AL/B1b-03 overlaps the field of Group 3 dikes (Fig. 4a), but we consider this to be a possible effect of hydrothermal alteration as it is among the most altered D-FP samples. The initial isotope composition of E-FP (radiogenic Nd, slightly radiogenic Sr and Pb, and radiogenic Os) shows general affinities towards the enriched mantle components (namely EM1 and EM2; Zindler and Hart, 1986; Hart, 1988; Shirey and Walker, 1998) and are most similar to those of the Paraná–Etendeka ferropicrites (Figs. 4–5; Os data not available). The high-Fe lavas of southern Lebombo (Fig. 1) are the closest isotopic correlates of E-FP within the Karoo province in terms of initial Sr and Nd isotopic composition

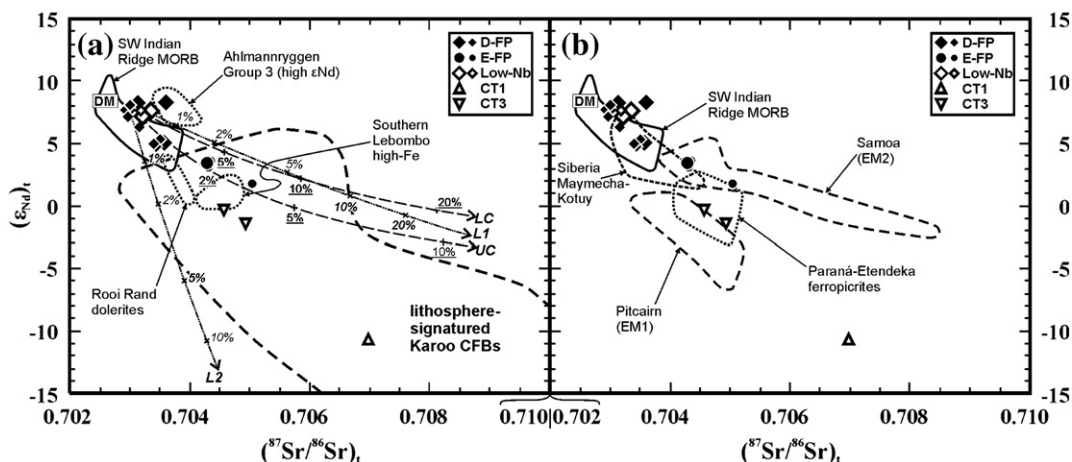


Fig. 4. Initial ϵ_{Nd} vs. $^{87}\text{Sr}/^{86}\text{Sr}$ of the Vestfjella samples in comparison with isotopic data for Rooi Rand dolerites, Karoo CFBs, and SW Indian Ridge MORBs (a) and some selected CFB-related rocks and oceanic basalts (b). Smaller symbols denote previously published data for D-FP, E-FP, and low-Nb type samples (Luttinen et al., 1998; Luttinen and Furnes, 2000; Heinonen and Luttinen, 2008). DM denotes average depleted MORB mantle of Workman and Hart (2005). All data calculated at 180 Ma, except for Paraná–Etendeka (132 Ma) and Siberia (250 Ma). In the case of SW Indian Ridge and DM, Pitcairn, and Samoa, the isotopic compositions of the mantle sources were back-calculated at 180 Ma using mantle reservoir compositions recommended by Workman and Hart (2005), Eisele et al. (2002), and Workman et al. (2004), respectively. Results of EC–AFC [with Archean crust (AC), average upper crust (UC), and average lower crust (LC) as contaminant end-members; Table 3] and AFC [with lithospheric mantle components (L1 and L2) as contaminant end-members; Table 4] modeling of a hypothetical primary D-FP melt shown in (a); tick marks indicate the amount of assimilated material relative to the original primary melt. References for a are Hawkesworth et al. (1984), Ellam and Cox (1989), Sweeney et al. (1994), Luttinen et al. (1998), Luttinen and Furnes (2000), Riley et al. (2005), and Jourdan et al. (2007a), and for b Woodhead and Devey (1993), Arndt et al. (1995), Gibson et al. (2000), Eisele et al. (2002), Workman et al. (2004), and Carlson et al. (2006). SW Indian Ridge MORBs compiled from the Petrological Database of the Ocean Floor (<http://www.petdb.org>).

(Fig. 4a). The range in initial isotopic compositions from D-FP to E-FP is largely similar to that found for meimechites and associated rocks of Maymecha–Kotuy region of the Siberian CFB province (Figs. 4–6; Carlson et al., 2006).

5.2. Other samples

The initial Sr and Nd isotopic compositions of the other Vestfjella samples also fall within or close to the ranges of the previously reported values for the different geochemical types (Fig. 4; cf. Luttinen et al., 1998; Luttinen and Furnes, 2000). The low-Nb type shows very unradiogenic initial $^{87}\text{Sr}/^{86}\text{Sr}$ (0.7032–0.7033) and radiogenic initial ϵ_{Nd} (+7.2 to +7.6) (Table 2; Fig. 4). CT3 exhibits more enriched compositions (initial $^{87}\text{Sr}/^{86}\text{Sr}$ = 0.7046–0.7049 and initial ϵ_{Nd} from –2.2 to –0.9) and CT1 shows highly radiogenic initial $^{87}\text{Sr}/^{86}\text{Sr}$ (0.7070) and unradiogenic initial ϵ_{Nd} (–10.7). Low-Nb sample 5-mk-91 is characterized by the most radiogenic initial Pb isotopic signature of the dataset with initial $^{206}\text{Pb}/^{204}\text{Pb}$ = 18.20, $^{207}\text{Pb}/^{204}\text{Pb}$ = 15.59, and $^{208}\text{Pb}/^{204}\text{Pb}$ = 38.31, whereas low-Nb sample P4-KHG-90 shows more unradiogenic values (17.67, 15.52, and 37.41, respectively) (Table 2; Fig. 5). Respective values are 17.28, 15.53–15.54, and 37.04–37.06 for CT3 and 17.01, 15.43, and 37.73 for CT1. The samples show a relatively restricted range of Os isotopic compositions: the low-Nb type shows slightly lower initial $^{187}\text{Os}/^{188}\text{Os}$ (0.1264–0.1286) relative to CT3 (0.1297–0.1308) and CT1 (0.1304) (Table 2; Fig. 6).

In comparison, the initial isotopic signature of the low-Nb type approaches values typical of SW Indian Ridge MORB and thus also D-

FP, although sample 5-mk-91 shows notably more radiogenic Pb isotopic compositions, at the limits of the values seen for SW Indian Ridge MORB (Figs. 4–6). The CT1 and CT3 lavas with relatively radiogenic initial Sr, and unradiogenic initial Nd, Pb, and Os show general isotopic similarity with the majority of lithosphere-signatured Karoo lavas (Figs. 4–6).

6. Discussion

6.1. The role of lithospheric mantle and crustal contamination

The isotopic data allows us to estimate the significance of the lithospheric contribution to the different Vestfjella magma types. The previously recognized within-group variation in initial Sr and Nd isotopic compositions in Gondwana-related flood basalts and extremely radiogenic Sr and unradiogenic Nd signatures have been associated with the involvement of subcontinental lithospheric mantle (SCLM) and/or crustal components (e.g., Faure et al., 1974; Hoefs et al., 1980; Hawkesworth et al., 1984; Hergt et al., 1991; Luttinen et al., 1998; Luttinen and Furnes, 2000; Jourdan et al., 2007a), but the relative contributions from these components have not been tightly constrained nor has the composition of magmas that may have been derived from melting below the lithosphere.

Compared to the common Karoo tholeiites, D-FP and the low-Nb types have isotopic compositions typical of oceanic basalts; in fact, they overlap the range of isotopic compositions observed for MORBs from the SW Indian Ridge (Figs. 4–5). This supports the previous interpretations that most of them represent relatively pristine

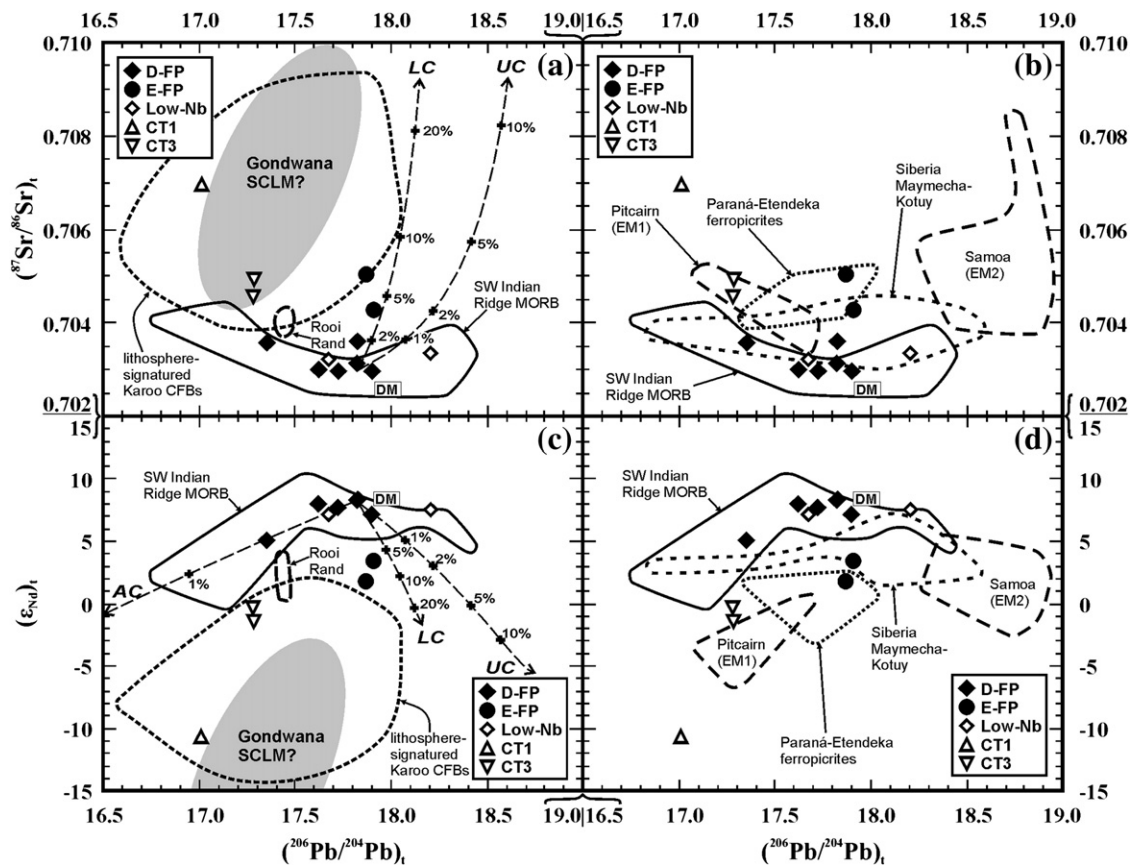


Fig. 5. Initial $^{87}\text{Sr}/^{86}\text{Sr}$ vs. $^{206}\text{Pb}/^{204}\text{Pb}$ (a, b), ϵ_{Nd} vs. $^{206}\text{Pb}/^{204}\text{Pb}$ (c, d), $^{207}\text{Pb}/^{204}\text{Pb}$ vs. $^{206}\text{Pb}/^{204}\text{Pb}$ (e, f), and $^{208}\text{Pb}/^{204}\text{Pb}$ vs. $^{206}\text{Pb}/^{204}\text{Pb}$ (g, h) of the Vestfjella samples in comparison with isotopic data for Rooi Rand dolerites ($n=2$ in a and c; $n=8$ in e and g), Karoo CFBs, and SW Indian Ridge MORBs (a, c, e, g) and some selected CFB-related rocks and oceanic basalts (b, d, f, h). DM and EC-AFC models (AC, UC, and LC) as in Fig. 4 (see Table 3 for parameters). All data calculated at 180 Ma, except for Paraná–Etendeka (132 Ma) and Siberia (250 Ma); for more details see Fig. 4. References for a, c, e, g are Hawkesworth et al., 1984; Betton et al. (1984), Ellam and Cox (1989, 1991), Smith (1983), Harmer et al. (1998), and Jourdan et al. (2007a), and for b, d, f, h Woodhead and Devey (1993), Eisele et al. (2002), Workman et al. (2004), Gibson et al. (2000), and Carlson et al. (2006). SW Indian Ridge MORBs compiled from the Petrological Database of the Ocean Floor (<http://www.petdb.org>).

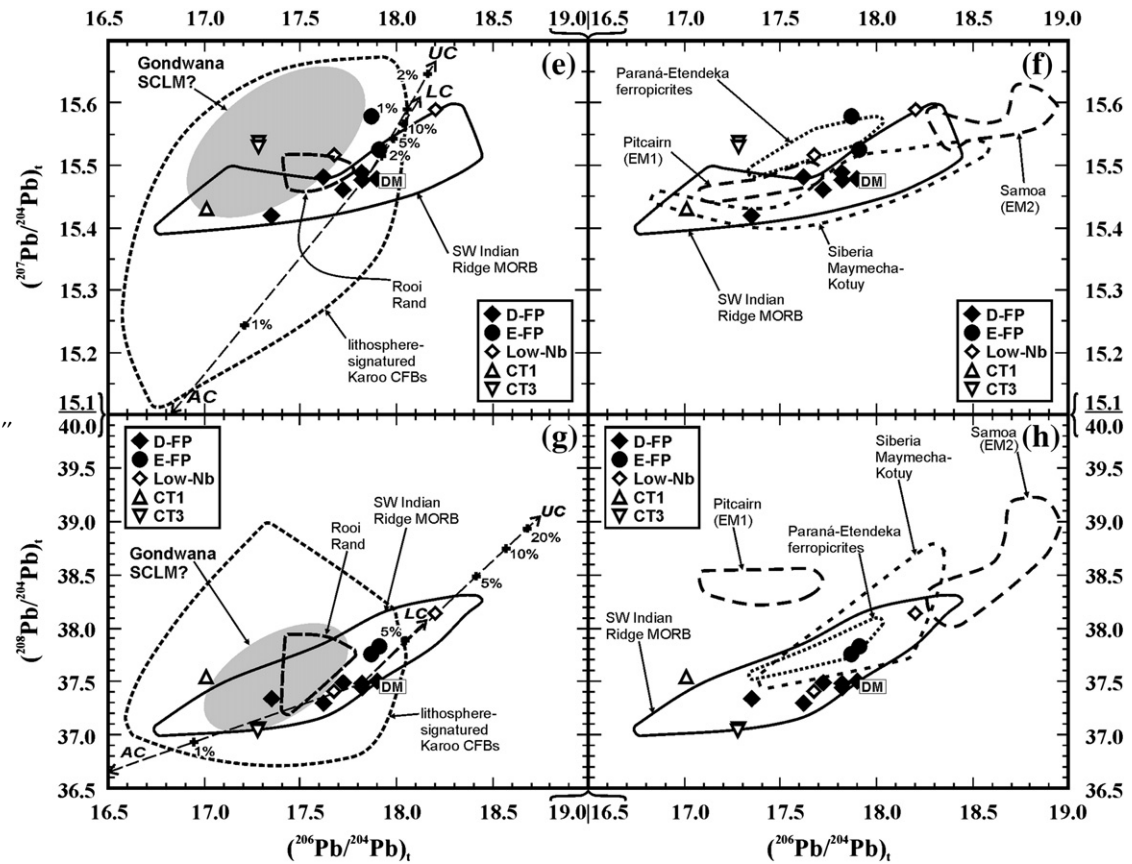


Fig. 5 (continued).

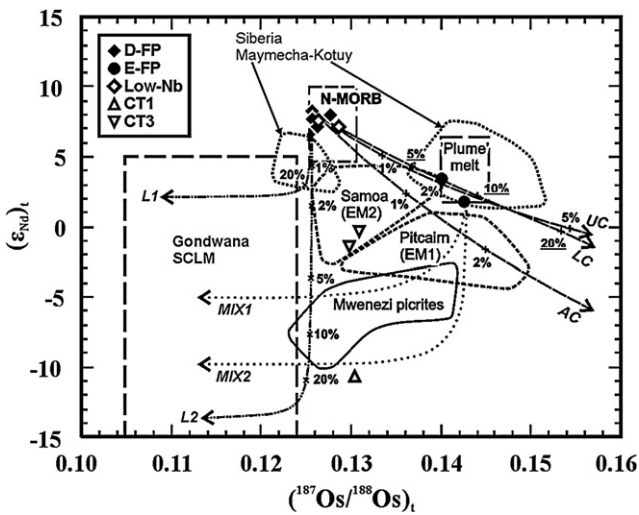


Fig. 6. Initial ϵ_{Nd} vs. $^{187}Os/^{188}Os$ diagram of the Vestfjella samples. Isotopic data for Mwenzei picrites (Ellam and Cox, 1989; Ellam et al., 1992), Pitcairn lavas (Woodhead and Devey, 1993; Eisele et al., 2002), Samoa lavas (Workman et al., 2004), and Siberia meimechites and related rocks (Horan et al., 1995; Carlson et al., 2006) shown for comparison. The composition of the Gondwana SCLM is estimated after Walker et al. (1989) and Simon et al. (2007). The Os isotopic compositions of N-MORB (based on abyssal peridotites) are estimated after Klein (2003) and Shirey and Walker (1998). 'Plume' melt-field after Ellam et al. (1992); MIX1 and MIX2 denote Karoo plume-lithosphere mixing models 1 and 3 of that study. EC-AFC models for crustal contaminants (AC, UC, and LC) and AFC models for lithospheric mantle contaminants (L1 and L2) are similar to Fig. 4 (see Tables 3 and 4 for parameters). All data calculated at 180 Ma, except for Siberia (250 Ma). In the case of MORB, Pitcairn, and Samoa, the Os isotopic compositions of the mantle sources were back-calculated at 180 Ma using $^{187}Re/^{188}Os$ ratios of 0.06 (MORB) and 0.4 (Pitcairn and Samoa) for the mantle reservoirs (cf. Shirey and Walker, 1998); Nd isotopic composition calculated as in Fig. 4.

sublithospheric mantle-derived magmas (Luttinen and Furnes, 2000; Heinonen and Luttinen, 2008) and, therefore, they provide a good starting point to investigate the effects of lithospheric contribution to other magma types.

We have modeled the contamination of a hypothetical D-FP parental magma with crustal components (Archean TTG, average upper and lower crust; Table 3; Figs. 4–7) and SCLM components (L1 and L2; Table 4; Figs. 4 and 6). We modeled crustal contamination as an EC-AFC process (Table 3; Bohrsen and Spera, 2001; Spera and Bohrsen, 2001). However, the lack of Os data on specific crustal components restricts the detailed modeling of Os and the calculated EC-AFC curves using average crustal values and estimated partition coefficients [parental magma $K_D(Os) = 1$; contaminant $K_D(Os) = 0.1$] should be considered tentative at best (Fig. 6). In addition, Sr isotopic data on the Kaapvaal-related Archean TTG has not been published and thus Sr was not modeled in its case (cf. Figs. 4 and 5a). Due to uncertainties regarding the nature of the lithospheric mantle, SCLM contamination was modeled as a more simplistic AFC process (DePaolo, 1981) in the case of Sr, Nd, and Os isotopic variation (Table 4; Figs. 4 and 6) by using SCLM partial melt compositions as contaminants. L1 and L2 represent isotopic extremes of Kaapvaal SCLM-derived partial melts and were selected in order to illustrate its compositional variability. Therefore, any mixing trend that is transitional between L1 and L2 is theoretically possible in the case of SCLM contamination. It should also be noted that metasomatic components in the lithospheric mantle, for example pyroxenitic veining, will have Os isotopic properties more similar to those of the average crustal components listed in Table 3. Consequently, if a sublithospheric melt were to preferentially incorporate such a metasomatic vein component, the mixing trends would roughly follow those for the crustal contamination trends shown in Fig. 6. Pb isotopes were not utilized in the AFC model due to limited amount of Pb data; the Pb isotopic composition of the Kaapvaal SCLM can only be tentatively

Table 3
Input parameters for the EC-AFC (Bohrson and Spera, 2001; Spera and Bohrson, 2001) models with crustal contaminants (Figs. 4–7).

Variable	PM [§]	Data source [*]	AC [§]	Data source [*]	UC [§]	Data source [*]	LC [§]	Data source [*]
Magma liquidus T (initial T) [°C]	1600	1	–	–	–	–	–	–
Assimilant liquidus T [°C]	–	–	1000	4	1000	4	1100	4
Assimilant initial T [°C]	–	–	300	4	300	4	600	4
Solidus T [°C]	–	–	900	4	900	4	950	4
Equilibration T [°C]	–	–	1100	Estimated; cf. 3	1100	Estimated; cf. 3	1100	Estimated; cf. 3
Isobaric specific heat [J/kg K]	1668	Calculated for PM; 1,3	1370	4	1370	4	1388	4
Crystallization enthalpy [J/Kg]	600,000	Calculated for PM; 1,3	–	–	–	–	–	–
Fusion enthalpy [J/Kg]	–	–	270,000	4	270,000	4	350,000	4
Sr [ppm]	188	AL/B9-03; 2	–	–	320	Continental UC; 9	348	Continental LC; 9
K _D (Sr)	0.0365	GERM	–	–	0.96	GERM	1.05	GERM
(⁸⁷ Sr/ ⁸⁶ Sr) _{180 Ma}	0.702962	AL/B9-03; Table 2	–	–	0.738470	Karoo model UC; 10	0.722231	Granulite 21BD6; 11
Nd [ppm]	11.15	AL/B9-03; 2	22	TTG sample 96/203; 5	27	Continental UC; 9	11	Continental LC; 9
K _D (Nd)	0.03961	GERM	0.136	GERM	0.136	GERM	0.19036	GERM
(¹⁴³ Nd/ ¹⁴⁴ Nd) _{180 Ma}	0.512829	AL/B7-03; Table 2	0.510551	TTG sample 96/203; 5	0.511800	Karoo model UC; 10	0.511806	Granulite 21BD6; 11
Pb [ppm]	0.93	AL/B9-03; Table 2	13	TTG sample 96/203; 5	17	Continental UC; 9	4	Continental LC; 9
K _D (Pb)	0.00311	GERM	0.584	GERM	0.584	GERM	0.427	GERM
(²⁰⁶ Pb/ ²⁰⁴ Pb) _{180 Ma}	17.818	AL/B7-03; Table 2	13.569	TTG sample 96/203; 5	18.83	Karoo model UC; 10	18.289	Granulite 21.1.89BD6; 12
(²⁰⁷ Pb/ ²⁰⁴ Pb) _{180 Ma}	15.489	AL/B7-03; Table 2	14.294	TTG sample 96/203; 5	15.89	Karoo model UC; 10	15.653	Granulite 21.1.89BD6; 12
(²⁰⁸ Pb/ ²⁰⁴ Pb) _{180 Ma}	37.48	AL/B7-03; Table 2	34.81	TTG sample 96/203; 5	39.19	Karoo model UC; 10	38.32	Granulite 21.1.89BD6; 12
Os [ppb]	2	Estimated; cf. Table 2	0.05	Continental UC; 7	0.05	Continental UC; 7	0.05	North Queensland LC; 13
K _D (Os)	1	Estimated	0.1	Estimated	0.1	Estimated	0.1	Estimated
(¹⁸⁷ Os/ ¹⁸⁸ Os) _{180 Ma}	0.12561	AL/B7-03; Table 2	2.5	Estimated; cf. 8	1.9	Continental UC; 7	0.8	North Queensland LC; 13
Nb [ppm]	3.46	AL/B9-03; 2	5	TTG sample 96/203; 5	12	Continental UC; 9	5	Continental LC; 9
K _D (Nb)	0.01843	GERM	0.28	GERM	0.28	GERM	0.35	GERM
Zr [ppm]	69	AL/B9-03; 2	132	TTG sample 96/203; 5	193	Continental UC; 9	68	Continental LC; 9
K _D (Zr)	0.076	GERM	0.145	GERM	0.145	GERM	0.23	GERM
Y [ppm]	12.81	AL/B9-03; 2	10	TTG sample 96/203; 5	21	Continental UC; 9	16	Continental LC; 9
K _D (Y)	0.0931	GERM	0.135	GERM	0.135	GERM	0.17	GERM

[§] PM = parental melt; AC = Archean crust; UC = average upper crust; LC = average lower crust.

^{*} Data sources (printed in bold and italics): 1 = Heinonen and Luttinen (2010); 2 = Heinonen and Luttinen (2008); 3 = Spera and Bohrson (2001); 4 = Bohrson and Spera (2001); 5 = Kreisssig et al. (2000); 6 = Luttinen and Furnes (2000); 7 = Esser and Turekian (1993); 8 = Dale et al. (2009); 9 = Rudnick and Gao (2003); 10 = Jourdan et al. (2007a); 11 = Talarico et al. (1995); 12 = Antonini et al. (1999); 13 = Saal et al. (1998); GERM = estimated from GERM database (<http://earthref.org/>).

constrained on the basis of published data on the nephelinites of the Buhera district in SE Zimbabwe (Harmer et al., 1998) and Group 2 kimberlites (Smith, 1983), and probably covers a much wider spectrum of values than shown in Fig. 5.

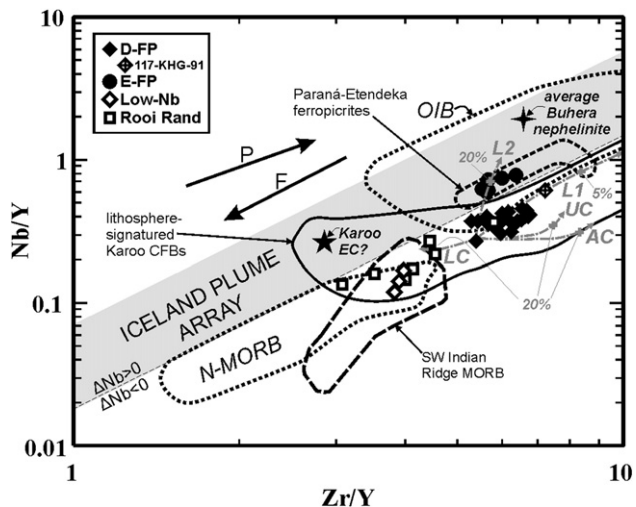


Fig. 7. Logarithmic Nb/Y vs. Zr/Y diagram of the D-FP, E-FP, low-Nb, and Rooi Rand dikes (data sources in addition to this study: Armstrong et al., 1984; Luttinen and Furnes, 2000; Heinonen and Luttinen, 2008). Data for lithosphere-signatured Karoo CFBs (approximated from GEOROC: <http://georoc.mpch-mainz.gwdg.de/georoc/>), SW Indian Ridge MORBs (compiled from the Petrological Database of the Ocean Floor; <http://www.petdb.org>), Paraná-Etendeka ferropicrites (Gibson et al., 2000), and average Buhera nephelinite (Harmer et al., 1998) shown for comparison. The Iceland Plume Array and fields for N-MORB and OIB after Fitton et al. (2003). Karoo EC represents hypothetical Nb-enriched end-member for the Karoo CFBs (cf. Section 6.3). P and F arrows denote the effect of increasing pressure and degree of melting, respectively (cf. Fitton et al., 1997). EC-AFC (AC, UC, and LC) and AFC (L1 and L2) models (gray curves) as in Fig. 4 (see Tables 3 and 4 for parameters). Tick marks denote the amount of assimilated material relative to the original primary melt (%).

The CT1 and CT3 magma types, used here as a reference data, plot in or close to the field of other major Karoo magma types in initial Sr, Nd, Pb, and Os isotopic space and show compositions that can be readily attributed to the contribution of lithospheric materials into these magmas (Figs. 4–6; cf. Luttinen et al., 1998; Luttinen and Furnes, 2000).

Although most of D-FP and low-Nb types show MORB-like isotopic signatures, the more evolved (MgO < 12 wt.%) samples, for example 117-KHG-91 with relatively radiogenic Sr and unradiogenic Nd and Pb initial isotopic composition (Table 2), could record incorporation of minor amounts (<2%) of SCLM and/or Archean crust into high- ϵ_{Nd} parental magma (Figs. 4–5; cf. Heinonen and Luttinen, 2008). In addition, the relatively high initial Pb isotope ratios of low-Nb type sample 5-mk-91 (Table 2) can be readily explained by minor *in-situ* contamination with the adjacent granite (cf. Fig. 5). Although we are not aware of the Pb isotope systematics of this granite (Pb = 24 ppm; O. T. Rämö, unpublished data), it bears evidence of a major Proterozoic crustal source component (Rämö et al., 2008) that is often associated with radiogenic Pb isotopic compositions (e.g., Rämö, 1991). Even very small amounts of contamination with this kind of material can effectively enrich the Pb isotopic composition of a primitive Pb-poor magma. Bearing this in mind, we suggest that the initial Pb isotopic composition of the sample P4-KHG-90 better represents that of the low-Nb type parental magmas.

The E-FP compositional type exhibits more radiogenic initial Sr, ²⁰⁷Pb, ²⁰⁸Pb, and Os, and less radiogenic initial Nd isotopic composition than D-FP (Table 2). Incompatible element pattern of E-FP also shows generally more enriched signature with higher La/Sm and Sm/Yb ratios, lower V/Lu ratio, and relative enrichment in Nb and Ta relative to D-FP (Fig. 3; Heinonen and Luttinen, 2008). It is important to note that D-FP parental magma *sensu stricto* cannot represent the uncontaminated parental magma for E-FP, because the significantly higher incompatible element contents (and, e.g., Sm/Yb ratios) of E-FP cannot be explained solely by reasonable degrees (<10%) of lithospheric contamination (and/or fractional crystallization) of a D-FP parental magma (cf.

Table 4

Input parameters for the AFC (DePaolo, 1981) models with lithospheric mantle contaminants (Figs. 4, 6, and 7).

Variable	PM [§]	Data source [*]	L1 [§]	Data source [*]	L2 [§]	Data source [*]
Rate of assimilation to crystallization is 0.5						
<i>Figure 4</i>						
Sr [ppm]	188	AL/B9-03; 1	3068	lamproite AL/KB8; 2	3068	lamproite AL/KB8; 2
K _D (Sr)	0.0365	GERM	–	–	–	–
(⁸⁷ Sr/ ⁸⁶ Sr) _{180 Ma}	0.702962	AL/B9-03; Table 2	0.708749 [†]	kimberlite Finsch B; 3	0.704989 [‡]	nephelinite ZCH-2; 4
Nd [ppm]	11.15	AL/B9-03; 1	229	lamproite AL/KB8; 2	229	lamproite AL/KB8; 2
K _D (Nd)	0.03961	GERM	–	–	–	–
(¹⁴³ Nd/ ¹⁴⁴ Nd) _{180 Ma}	0.512829	AL/B7-03; Table 2	0.512275 [†]	kimberlite Finsch B; 3	0.511414 [‡]	nephelinite ZCH-2; 4
<i>Figure 6</i>						
Os [ppb]	2	estimated;cf. Table 2	0.5	Karoo model; 5	0.5	Karoo model; 5
K _D (Os)	1	estimated	–	–	–	–
(¹⁸⁷ Os/ ¹⁸⁸ Os) _{180 Ma}	0.12561	AL/B7-03; Table 2	0.10927	xenolith 1107; 6	0.11399	xenolith K21; 7
Nd [ppm]	11.15	AL/B9-03; 1	229	lamproite AL/KB8; 2	229	lamproite AL/KB8; 2
K _D (Nd)	0.03961	GERM	–	–	–	–
(¹⁴³ Nd/ ¹⁴⁴ Nd) _{180 Ma}	0.512829	AL/B7-03; Table 2	0.512501	xenolith 1107; 6	0.511652	xenolith K21; 7
<i>Figure 7</i>						
Nb [ppm]	3.46	AL/B9-03; 1	170	lamproite AL/KB8; 2	33	avg nephelinite; 4
K _D (Nb)	0.01843	GERM	–	–	–	–
Zr [ppm]	69	AL/B9-03; 1	1076	lamproite AL/KB8; 2	112	avg nephelinite; 4
K _D (Zr)	0.076	GERM	–	–	–	–
Y [ppm]	12.81	AL/B9-03; 1	37	lamproite AL/KB8; 2	17	avg nephelinite; 4
K _D (Y)	0.0931	GERM	–	–	–	–

[§] PM = parental melt; L1 = Lithospheric mantle contaminant 1; L2 = Lithospheric mantle contaminant 2 (see Section 6.1).^{*} Data sources (printed in bold and italics): 1 = Heinonen and Luttinen (2008); 2 = Luttinen et al. (2002); 3 = Smith (1983); 4 = Harmer et al. (1998); 5 = Ellam et al. (1992); 6 = Walker et al. (1989); 7 = Simon et al. (2007); GERM = estimated from GERM database (<http://earthref.org/>). [†] Calculated at 118 Ma (cf. Smith, 1983). [‡] Calculated at 190 Ma (cf. Harmer et al., 1998).

Heinonen and Luttinen, 2008). Nevertheless, this alone does not rule out the possibility that they shared a common mantle source; perhaps the E-FP parental magmas initially were compositionally distinct from D-FP, because they represent lower degrees of melting of the same source. In comparison, D-FP sample 117-KHG-91, considered to represent a slightly contaminated (see above) low-degree melt from D-FP sources (Heinonen and Luttinen, 2008), has high La/Sm and Sm/Yb ratios similar to E-FP (Fig. 3; Heinonen and Luttinen, 2008), but it exhibits the characteristic low Nb, low Ta, and high V/Lu of D-FP (Fig. 3). In theory, the hypothetical uncontaminated parental melt of E-FP could exhibit compositional characteristics transitional between 117-KHG-91 and common D-FP signature.

Although contamination of a D-FP source parental magma with crustal material (<10%) can produce a rock with somewhat similar isotopic composition to E-FP (Figs. 4–6), some distinct trace element characteristics cannot be the result of such process. Continental crust is characterized by very low Nb and Ta contents (Rudnick and Gao, 2003) and, e.g., the higher Nb/Y of E-FP at a given Zr/Y (Fig. 7) is very difficult to explain by any amount of crustal addition into a parental melt derived from the D-FP sources at different pressures and/or degrees of melting (Fig. 7; cf. Fitton et al., 1997). In comparison, effects of varying melting conditions (and minor lithospheric contamination) on Nb–Zr–Y systematics are exemplified by the sample 117-KHG-91 derived from D-FP sources by lower degree of melting (Figs. 3 and 7; cf. Heinonen and Luttinen, 2008). Even if the isotopic compositions of E-FP could be explained by minor crustal contamination of a D-FP parental magma, the magmas must have experienced Nb and Ta enrichment by some other process.

Could SCLM contamination of D-FP-source magma then result in E-FP signature? First, the radiogenic Os of E-FP excludes bulk SCLM as an important mixing component because this would drive the Os isotopic composition to less radiogenic values (Fig. 6). On the other hand, the relatively low, OIB-like Os contents (0.2–0.3 ppb; Table 2) of E-FP renders their Os isotope systematics highly susceptible to very low degrees of crustal contamination if the contaminant has relatively high Os contents (e.g. >0.03 ppb) and highly radiogenic ¹⁸⁷Os/¹⁸⁸Os (e.g. >1). If the EC-AFC process is considered, less than 1% of

contamination would be able to move the ¹⁸⁷Os/¹⁸⁸Os of E-FP to highly enriched values (>0.15). Such contamination would not be easily detectable in trace element and Sr, Nd, and Pb isotope composition and thus poses a possible problem in interpreting the Os signature of E-FP. If the high initial ¹⁸⁷Os/¹⁸⁸Os of E-FP is a mantle-derived primary signature, however, it is particularly important because it lies outside the range usually observed for mantle peridotites (0.11–0.13; Shirey and Walker, 1998; Chesley et al., 2004), although in some rare occasions, values up to 0.15 have been reported in highly metasomatized peridotites (e.g., Lee et al., 2000). Simon et al. (2007) speculate that the Kaapvaal SCLM could have been locally metasomatized by fluids derived from ancient subducted sediments that carry highly radiogenic ¹⁸⁷Os/¹⁸⁸Os. Not only such fluids are unlikely to significantly affect the signature of Os-rich mantle peridotites (Chesley et al., 2004), however, but they are also likely to exhibit negative Nb (and Ta) abundance anomalies (e.g., Keppler, 1996), on the contrary to E-FP (cf. Fig. 3). Furthermore, mixing with a low-degree melt of the peridotitic SCLM, depicted by the mixing trend with lamproitic melt in Fig. 7, cannot account for high Nb/Y either. Importantly, the Vestfjella lamproite used in the model exhibits higher Nb/Y (4.6) and lower Zr/Y (29) relative to average lamproite (3.5 and 34, respectively; Bergman, 1987). One way to obtain radiogenic Os in SCLM is to involve pyroxene-rich components that derive from the crystallization of infiltrating magmas (i.e. melt metasomatism) in lithospheric mantle peridotite (e.g., Carlson and Nowell, 2001). Some kimberlites that intrude the Kaapvaal craton contain pyroxenitic xenoliths that exhibit ¹⁸⁷Os/¹⁸⁸Os up to 0.14 at 180 Ma (Olive et al., 1997). Mixing with (or derivation from) such pyroxenitic SCLM components with possibly even higher ¹⁸⁷Os/¹⁸⁸Os could result in radiogenic Os signature observed in E-FP. Importantly, such melt component, that is enriched in not only fluid-mobile, but also fluid-immobile incompatible elements (e.g., Wang et al., 2008), could also theoretically explain the elevated Nb and Ta content of E-FP as well as relatively unradiogenic Nd isotopic composition. For example, nephelinites from the Buhara district have been thought to derive from enriched (pyroxenitic?) SCLM and exhibit relatively high Nb contents (Fig. 7; Harmer et al., 1998).

Unfortunately, representative compositions for such pyroxenitic SCLM contaminants are very difficult to constrain. Moreover, given the very high concentrations of Os in the surrounding peridotite, the interaction should have been strictly limited to the pyroxenitic components. It is important to note that pyroxenitic veining is also possible in sublithospheric mantle, so distinguishing whether such a contribution was added to the E-FP magmas through lithospheric contamination or as a component of their sublithospheric source is difficult to impossible.

In summary, Sr, Nd, Pb, and Os isotope systematics of D-FP and the low-Nb types indicate that the role of lithospheric contamination in their petrogenesis was negligible, although some of the more evolved samples (i.e. MgO < 12 wt.%) and low-Nb sample 5-mk-91 have probably been subjected to minor contamination. Although derivation of E-FP from D-FP sources by lower degree melting and by subsequent lithospheric mantle contamination could be theoretically possible on the basis of their isotope systematics (Figs. 4–6), some crucial trace element ratios (such as high Nb/Y at a given Zr/Y; Fig. 7) indicate that either the possible contaminant must have been of anomalous composition (e.g., pyroxenite veins in SCLM) or the E-FP parental magmas were at least partly derived from anomalous enriched sublithospheric mantle components. The case of E-FP is further complicated by the fact that this chemical type consists of only two dikes and, unlike in the case of many extensively sampled volcanic rock series, examination of possible isotopic mixing trends and identification of possible distinct end-members is not currently possible.

6.2. Sublithospheric mantle sources

6.2.1. Mantle sources of the Vestfjella depleted types (D-FP and the low-Nb types)

The similar initial isotopic signatures (radiogenic Nd, unradiogenic Sr, Pb, and Os) of D-FP and the low-Nb types suggest that they were derived from similar depleted mantle sources (Figs. 4–6). This is also supported by their trace element signatures that show depletion of the highly incompatible elements (Fig. 3). The MORB-like isotopic signatures (Figs. 4–6) of the Vestfjella depleted types and the highly magnesian compositions of their parental magmas (MgO up to 25 wt.%; Heinonen and Luttinen, 2010) are compatible with sources that, unlike proposed initially (cf. Heinonen and Luttinen, 2008), do not contain significant amounts of recycled crustal materials. Although crustal materials may exhibit low Rb/Sr, U/Pb, Th/Pb, and high Sm/Nd ratios (e.g., Klein, 2003) and thus generate relatively unradiogenic Sr, Pb, and radiogenic Nd isotopic signatures with time, Re/Os ratios in them are invariably high (e.g., Shirey and Walker, 1998) and should result in radiogenic Os isotopic signatures in the recycled crustal component (cf. Sobolev et al., 2008); such radiogenic Os is not observed in the Vestfjella depleted types (Fig. 6). It should be noted, however, that many Indian Ocean MORBs show anomalous isotope and trace element characteristics relative to Atlantic and Pacific MORBs in general (e.g., slightly higher $^{87}\text{Sr}/^{86}\text{Sr}$ and lower $^{206}\text{Pb}/^{204}\text{Pb}$, ϵ_{Nd} , and ϵ_{Hf}) — a feature that has been thought to indicate large-scale entrainment of minor proportions of recycled lithospheric components in the depleted upper mantle beneath the Indian Ocean (e.g., Mahoney et al., 1992; Rehkämper and Hofmann, 1997; Janney et al., 2005; Nishio et al., 2007). Accordingly, there is a possibility that such diluted recycled components were also involved in the genesis of the Vestfjella depleted types. Nevertheless, the aforementioned major element and isotope characteristics indicate a principal long-term depleted peridotitic mantle source.

Whether the source of the Vestfjella depleted types resided in the lower or upper mantle is an important question. First, the high T_p values (> 1600 °C) estimated for the sources of the meimechites are at least ~200 °C higher compared to the ambient mantle (e.g., Putirka, 2008) and associate the depleted types with hotspot-related

magmatic activity (Heinonen and Luttinen, 2010). Although the isotopic compositions of the Vestfjella depleted types are very similar to SW Indian Ridge MORB and distinct from hotspot-related OIBs in general (Figs. 4–6), strongly depleted isotopic signatures are also seen in many hotspots that are believed to represent surface manifestations of mantle plumes, e.g., Iceland (Kerr et al., 1995; Fitton et al., 2003). This does not strictly mean that the depleted source is an intrinsic part of the plume itself (i.e., in the form of entrained lower mantle or, e.g., recycled oceanic lithosphere; cf. Kerr et al., 1995), because MORB-source upper mantle may be entrained in plumes during their ascent (e.g., Richards and Griffiths, 1989).

The distinct major and trace element characteristics of D-FP and MORB do not necessarily exclude derivation from a similar mantle source. For example, the relatively high MgO (25 wt.%) and FeO_{tot} (12–13 wt.%) and low Al_2O_3 (7 wt.%) of the calculated D-FP parental magmas can be explained by relatively low-degree melting of depleted peridotite at high pressures (5–6 GPa; Heinonen and Luttinen, 2010; cf. Herzberg and O'Hara, 2002). Some of the OIB-like trace element characteristics [e.g., high Zr/Y = 5–6 and $(\text{Sm}/\text{Yb})_{\text{N}} = 3–5$; Fig. 3] can also be attributed to relatively low degrees of melting at high pressures in the presence of garnet that has high $K_d^{\text{grt-liq}}$ values for Y and HREE (cf. Fig. 7). The same may apply to the positive V anomalies [primitive mantle-normalized $(\text{V}/\text{Lu})_{\text{PMN}} = 1.8–2.2$; Fig. 3] that were previously considered as indicators of recycled oceanic gabbros (Heinonen and Luttinen, 2008): experiments have shown that garnet has notably higher K_d values for, e.g., Yb (6.6) and Lu (7.1) compared to V (3.8) at high pressures (Johnson, 1998). In addition, the study of Adam and Green (2006) showed that $K_d(\text{V})^{\text{crystal-liq}}$ values decline in clinopyroxene, mica, and amphibole with increasing pressure and temperature, whereas, e.g., $K_d(\text{Lu})^{\text{crystal-liq}}$ remain relatively constant. The aforementioned relationships are exemplified by the low-Nb type that exhibits major and trace element characteristics [e.g., $\text{FeO}_{\text{tot}} = 11–12$ wt.%, $\text{Al}_2\text{O}_3 = 10–12$ wt.%, Zr/Y = 4, $(\text{Sm}/\text{Yb})_{\text{N}} = 2–3$, $(\text{V}/\text{Lu})_{\text{PMN}} = 1.4–1.5$] that are intermediate between D-FP and average MORB [e.g., $\text{FeO}_{\text{tot}} = 9$ wt.%, $\text{Al}_2\text{O}_3 = 16$ wt.%, Zr/Y = 3, $(\text{Sm}/\text{Yb})_{\text{N}} = 1$, $(\text{V}/\text{Lu})_{\text{PMN}} = 0.5$; Salters and Stracke, 2004]. These characteristics imply that the parental magmas of the low-Nb type were generated at lower pressures and at higher degrees of melting relative to those of D-FP, but at higher pressures and lower degrees of melting relative to those of MORBs.

Fitton et al. (1997, 2003) used the combination of Nb/Y and Zr/Y ratios (Fig. 7) in order to distinguish relatively Nb-enriched plume sources from ambient MORB sources in Iceland. MORB unanimously show $\Delta\text{Nb} < 0$ [$\Delta\text{Nb} = 1.74 + \log(\text{Nb}/\text{Y}) - 1.92 \log(\text{Zr}/\text{Y})$] compatible with Nb-poor upper mantle sources whereas Icelandic lavas exhibit $\Delta\text{Nb} > 0$ indicating relatively Nb-enriched (plume?) sources (Fig. 7; e.g., Fitton et al., 1997). The low-Nb type [$\Delta\text{Nb} = -0.2 - (-0.3)$] plots within the MORB field and, although D-FP [$\Delta\text{Nb} = -0.1 - (-0.3)$] shows relatively higher Nb/Y and Zr/Y ratios and partially overlap the low-Nb/Y portion of the OIB field, lower degrees of melting of the MORB source at higher pressures to produce the D-FP signature could again readily explain these differences (Fig. 7). In summary, there is no trace element or isotopic evidence that would indicate plume-like sources for the Vestfjella depleted types and, instead, strongly point to their derivation from MORB-like upper mantle sources.

The relatively high water contents postulated on the parental magmas of D-FP ($\text{H}_2\text{O} \approx 1–2$ wt.%; Heinonen and Luttinen, 2010), however, are difficult to explain simply by low-degree, high-pressure melting of a common MORB peridotite source. Given that the compatibility of water in peridotite is about 0.5–1 times that of Ce (Hauri et al., 2006) and that the range of water content in the depleted mantle is 70–160 ppm (Workman and Hart, 2005), partial melting of less than 1% is required to produce 1 wt.% of water in the melt. Given the subalkaline nature of the magmas, this is unacceptably low and indicates that the mantle source was enriched in water relative to DM. Wet ultramafic magmas from otherwise depleted mantle sources

have also been described from, e.g., the Archean Kaapvaal Craton, where their high water contents have been ascribed to second-stage enrichment by subduction processes (Wilson et al., 2003). Moreover, the source of water in the Paleoproterozoic Pechenga ferropicrites has been speculated to be either a metasomatized subcontinental mantle or a volatile-bearing plume (Fiorentini et al., 2008). Although we have no straightforward means to differentiate between these alternatives, the subduction-sensitive trace element ratios (e.g., Ba/Nb and U/Nb) of the Vestfjella depleted types (10–20 and 0.02–0.03, respectively; Table 1) are slightly higher than in average N-MORB (3 and 0.02, respectively; Sun and McDonough, 1989) and more alike those of Indian Ocean MORB (1–20 and 0.02–0.03, respectively; e.g., le Roex et al., 1989; Rehkämper and Hofmann, 1997). Consequently, recycling processes, such as those associated with the mildly LILE-enriched Indian Ocean MORB source (cf. Rehkämper and Hofmann, 1997; Janney et al., 2005; Nishio et al., 2007), may have added water into the mantle sources of the Vestfjella depleted types.

In the light of the current data, we envisage that the Vestfjella depleted types were generated by deep melting of heated, depleted upper mantle that was enriched in water either by subduction/metamorphism processes or by a plume. There is no geochemical evidence that would indicate that the source of the Vestfjella depleted types was related to the purported plume itself, unless the plume had chemical and isotopic characteristics similar to the source of Indian Ocean MORB.

6.2.2. Sublithospheric mantle sources of E-FP

Although the geochemical and isotopic characteristics of E-FP could theoretically be explained by contamination of a D-FP-like parental magma with pyroxenite veins in SCLM (or by direct derivation from them; Section 6.1.), it is important to note that such components may also be present in the sublithospheric mantle. The relative Nb and Ta enrichment and the overall geochemical and Sr, Nd, Pb, and Os isotopic similarity to EM-like OIBs (Figs. 3–7; cf. Heinonen and Luttinen, 2008) could indicate the involvement of recycled lithospheric materials, e.g., sediment-bearing oceanic crust (e.g., White and Hofmann, 1982; Hauri and Hart, 1993; Reisberg et al., 1993; Eisele et al., 2002; Jackson and Dasgupta, 2008; Jackson et al., 2008; Sobolev et al., 2008). To further test this possibility, we used a spreadsheet provided by Stracke et al. (2003) for modeling the Sr, Nd, and Pb isotopic evolution of mantle sources that entrain recycled oceanic crust (Fig. 8; electronic Appendix B). Due to obvious uncertainties related to the initial concentrations, isotopic compositions, and behavior of Re and Os (Stracke et al., 2003; cf. Carlson, 2005), the spreadsheet did not include Os isotopes. We used the standard parameters recommended by Stracke et al. (2003) and only altered the recycling age and the relative amount of subducted sediment and igneous crust in the calculations (electronic Appendix B). The results of our calculations indicate that the presence of recycled oceanic crust with recycling age of ~0.8 Ga and containing ~5–15 vol.% of sediment material (GLOSS; Plank and Langmuir, 1998)

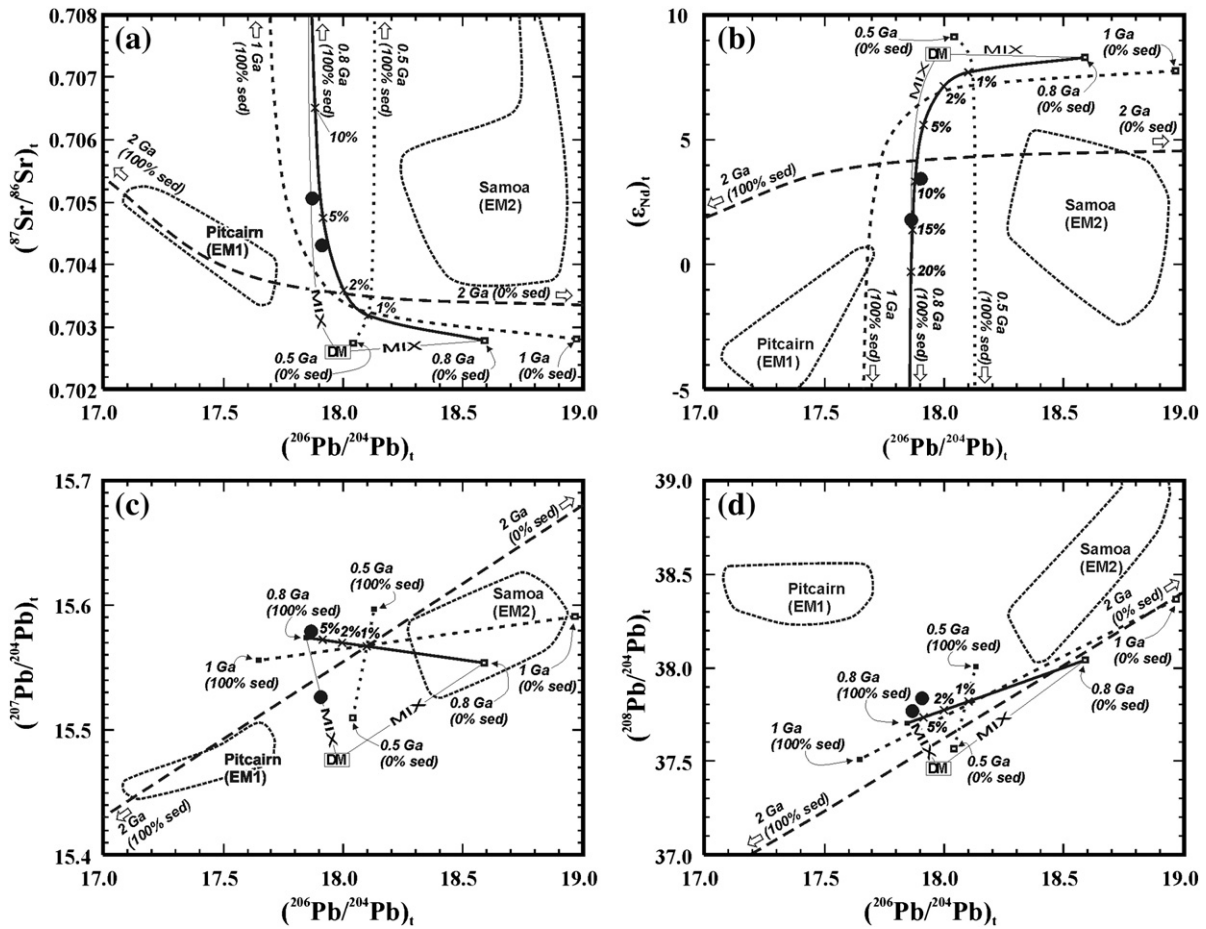


Fig. 8. The isotopic compositions of E-FP and the results of isotopic modeling of mantle reservoirs that consist of recycled oceanic crust shown in initial $^{87}\text{Sr}/^{86}\text{Sr}$ vs. $^{206}\text{Pb}/^{204}\text{Pb}$ (a), ϵ_{Nd} vs. $^{206}\text{Pb}/^{204}\text{Pb}$ (b), $^{207}\text{Pb}/^{204}\text{Pb}$ vs. $^{206}\text{Pb}/^{204}\text{Pb}$ (c), and $^{208}\text{Pb}/^{204}\text{Pb}$ vs. $^{206}\text{Pb}/^{204}\text{Pb}$ (d) diagrams. Isotopic data for Pitcairn and Samoa lavas and average depleted MORB mantle (DM) shown for comparison (cf. Fig. 5). All data calculated at 180 Ma (cf. Figs 4 and 5). 0.5 Ga, 0.8 Ga, 1 Ga, and 2 Ga indicate recycling ages for the modeled reservoirs. Percentages indicate the relative amount of sediment in the recycled oceanic crustal component; percentages of 1–20% with tick marks only shown for 0.8 Ga recycled crust. MIX-paths denote binary mixing curves between ADM and 0.8 Ga recycled end-members. See electronic Appendix B and Stracke et al. (2003) for model parameters.

in the source could theoretically explain the Sr, Nd, and Pb isotope characteristics of E-FP (Fig. 8). The disadvantage of these kinds of calculations is that they are not very well constrained (cf. Stracke et al., 2003). Without question, further studies of complex processes that take place during alteration and subduction (e.g., Kelley et al., 2005), and those that take place subsequently in the mantle (e.g., Kogiso et al., 1997), are needed until isotope compositions of OIB-like volcanic rocks can be convincingly linked to specific recycled crustal materials (Stracke et al., 2003; cf. Niu and O'Hara, 2003).

Due to the numerous uncertain geochemical factors related to the modeling of lithospheric contamination and recycling, the definite nature of the E-FP sources will remain uncertain. Nevertheless, the general geochemical composition, (Heinonen and Luttinen, 2008) and relatively high initial $^{187}\text{Os}/^{188}\text{Os}$ associate E-FP with pyroxenitic or pyroxenite-bearing mantle components, that were also indicated for geochemically and isotopically similar Paran -Etendeka ferropicrites (Figs. 4 and 5; Gibson et al., 2000; Tuff et al., 2005).

6.3. Relationships with Karoo magmatism

One of the most important questions regarding the implications of low-Nb, D-FP, and E-FP magma types is their relationships with Karoo magmatism: are their sources significant Karoo end-members or just anomalous heterogeneities that had little to do with the Karoo in general? Obviously, the strong lithospheric signature of the majority of Karoo magma types makes exploring different possibilities a difficult task at best. In addition, there is no age data on the Vestfjella dikes which restricts the evaluation of their temporal position relative to Karoo main pulse at ~180 Ma.

The OIB-like trace element and isotope characteristics of E-FP are not known elsewhere in the Karoo province, although the high-Fe lavas of southern Lebombo have been speculated to represent contaminated differentiates of E-FP-source magmas (Fig. 4a; Heinonen and Luttinen, 2008). On the other hand, the "plume–lithosphere" mixing curve of Ellam et al. (1992), reconstructed on the basis of Nd–Os isotope systematics of the Mwenezi picrites, indicates that the postulated Karoo "plume end-member" closely corresponds to the E-FP source component (Fig. 6). The nature of the "plume end-member" is not well constrained (Ellam et al., 1992), however, and the Mwenezi picrites have also been connected to MORB source and heterogeneous lithospheric mantle end-members (Ellam and Cox, 1991; Ellam, 2006). Importantly, the Nb systematics [$\Delta\text{Nb} = -0.2 - (-0.7)$] of the Mwenezi picrites do not imply the involvement of OIB-like components. Probably the closest correlatives of E-FP within the Gondwana framework are the ferropicrites of the Paran -Etendeka CFB province (Fig. 1). Given the major and trace element (Heinonen and Luttinen, 2008; Fig. 7) as well as isotopic similarity (Figs. 4–5), we have reasons to suggest that these primitive magma types, separated by ~50 Ma in age and by ~6000 km distance at present, sampled very similar pyroxenitic components in the deep sub-Gondwanan mantle (cf. Gibson et al., 2000; Thompson et al., 2001; Tuff et al., 2005). Such enriched components may well represent small-scale heterogeneities that are insignificant in flood basalt generation in general (cf. Gibson et al., 2000; Heinonen and Luttinen, 2008). On the other hand, some Karoo CFBs show relatively high ΔNb (up to 0.5) at low Zr/Y indicative of anomalous enriched sources (Fig. 7). In theory, this same Nb-enriched source may have been sampled by E-FP at higher pressures and lower degrees of melting (cf. Fig. 7). It should be noted that relative Nb-enrichment is difficult to explain by contamination with crustal materials or involvement of metasomatized lithospheric peridotite (Fig. 7; cf. Section 6.1.).

The Vestfjella depleted types, and namely D-FP, have been associated with anomalously high sublithospheric mantle potential temperatures (>1600 °C) and pressures (5–6 GPa; depth of ~150–200 km) (Heinonen and Luttinen, 2010). Such extreme conditions are compatible with the very high melting rates needed for the formation of flood basalts. Moreover, the geochemical association of the low-Nb type with Vestfjella

lavas (cf. Luttinen and Furnes, 2000) indicates that such depleted MORB-like sources were involved in the generation of the Karoo CFBs. In comparison with the majority of Karoo magma types, the Vestfjella depleted types show highly depleted initial Sr and Nd isotopic composition (Fig. 4a). The Group 3 dikes from Ahlmannryggen show equally radiogenic initial ϵ_{Nd} , but their generally higher initial $^{87}\text{Sr}/^{86}\text{Sr}$ and significant LREE depletion [$(\text{La}/\text{Sm})_{\text{N}} < 1$] associated with significant enrichments in HFSE (e.g., $\text{TiO}_2 = 3\text{--}4$ wt.%) indicate that they sample a distinctive source component that is not related to Vestfjella dikes or other Karoo magma types (Fig. 4a; Riley et al., 2005; Jourdan et al., 2007a). The MORB-like Rooi Rand dikes have been previously connected with the low-Nb type (cf. Luttinen and Furnes, 2000), but detailed comparison is hampered by inadequate isotopic and geochemical data (cf. Figs. 4, and 5a, c). Nevertheless, the Rooi Rand dikes show significant geochemical heterogeneity (Armstrong et al., 1984; cf. Fig. 7), and given, e.g., the relatively high variation in La/Sm (1.3–2.7; Duncan et al., 1990) and low initial ϵ_{Nd} values (Fig. 4; Hawkesworth et al., 1984), some of them may have been subjected to minor lithospheric contamination. Nevertheless, their low ΔNb [$-0.1 - (-0.2)$; Armstrong et al., 1984] and Pb isotope systematics (Betton et al., 1984) suggest that they may well be related to similar asthenospheric upper mantle sources that produced the Vestfjella depleted types (Luttinen and Furnes, 2000; cf. Figs. 6e,g and 7). On the other hand, their significantly lower $(\text{Sm}/\text{Yb})_{\text{N}}$ values (≤ 2) relative to, e.g., D-FP (3–5) indicate their derivation beneath already significantly thinned lithosphere, compatible with them erupting a few million years after the peak of Karoo magmatism (cf. Duncan et al., 1990; Jourdan et al., 2007a,b).

In summary, given that the major and trace element characteristics of the Vestfjella depleted types are attributable to melting of a 'common' peridotite at great depths and temperatures (Heinonen and Luttinen, 2010; cf. Fig. 7) and that the isotope and trace element systematics of many of the Karoo CFBs could be explained by lithospheric contamination of such MORB-source magmas (Figs. 4, 5, and 7; cf. Luttinen and Furnes, 2000), we suggest that the Vestfjella depleted types sampled a significant depleted sublithospheric end-member for Karoo magmatism, rather than were derived from some hot, anomalous MORB-like upwelling that post-dated the peak of Karoo magmatism (cf. Section 6.4.). We emphasize that it is still very likely that some (or even most) of the Karoo magmas were generated within the lithosphere (cf. Jourdan et al., 2007a), but, on the other hand, our results cast serious doubts on models that suggest such origin for all of them (e.g., Hawkesworth et al., 1984; Elburg and Goldberg, 2000; Scenario 1 of Jourdan et al., 2007a).

6.4. Implications for the generation of the Karoo CFB province and the break-up of Gondwana

Our study indicates that the mantle sources of the highly magnesian dikes of Vestfjella contained both depleted and enriched components. In the following text, we speculate on the implications of our findings for the origin of the Karoo CFBs and the break-up of Gondwana in general.

One of the most important aspects in the petrogenesis of the depleted ferropicrites and meimechites are the high mantle potential temperatures (>1500–1600 °C) required for their generation (Heinonen and Luttinen, 2008, 2010). These temperatures are well over that of ambient mantle (~1400 °C; e.g., Putirka, 2008) and require that a significant thermal anomaly existed in the sub-Gondwanan mantle. The only CFB models that propose increased mantle temperatures are the "active" plume model (Fig. 9a; e.g., Morgan, 1971) and the "passive" internal mantle heating model ("mantle global warming"; Fig. 9b; Gurnis, 1988; Coltice et al., 2007), both of which have been used to explain the Karoo volcanism (e.g., Richards et al., 1989; Coltice et al., 2009; respectively). Mantle potential temperatures up to 1700 °C have been suggested for plumes (e.g., Thompson and Gibson, 2000) and recent estimates of the thermal effect of a thick lithospheric lid suggest asthenospheric mantle temperatures up to ~1600 °C in a single supercontinent model (Coltice et al., 2007). With increasing number of continents (≥ 2), temperatures

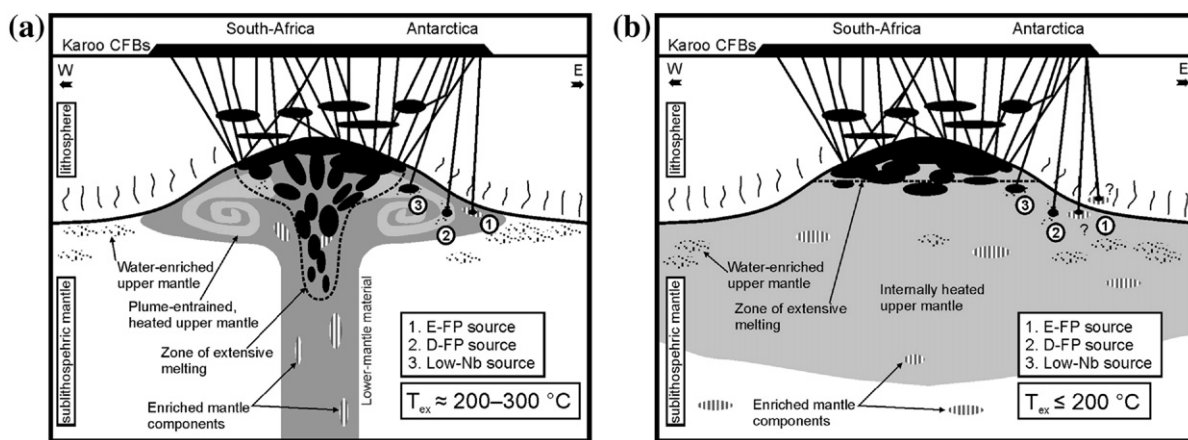


Fig. 9. Schematic presentations of a plume model (a) and an internal mantle heating model (b) to explain the generation of the Karoo CFBs (see Section 6.4). T_{ex} denotes the approximate maximum temperature difference between the gray area and the ambient mantle. We emphasize that T_{ex} of at least ~ 100 – 200 is needed in order to generate ferropicritic and meimechitic magmas, respectively (cf. Gibson et al., 2000; Elkins-Tanton et al., 2007; Heinonen and Luttinen, 2008, 2010). T_{ex} values in a after Putirka (2008) and in b after Coltice et al. (2007).

in the internal heating model decrease from ~ 1500 °C to close to that of the ambient mantle (Coltice et al., 2007).

Mantle plume and internal heating models for the generation of the Karoo CFBs are compared visually in Fig. 9. In the mantle plume model the source of the Vestfjella depleted types represents plume-entrained, heated upper mantle that was hydrated. The source of E-FP represents an enriched mantle component carried within the plume (Fig. 9a). In the internal heating model both components are intrinsic to the upper mantle (Fig. 9b). What is common to both scenarios is that, whereas the majority of the Karoo parental melts form within the low-pressure melting regime just below and within the lithosphere, the primary magmas of the Vestfjella depleted types and E-FP form at greater depths in the subcontinental mantle: their sources were either hydrous (depleted types) or fertile in general (E-FP) and thus likely susceptible to partial melting at greater depths relative to the surrounding mantle (Heinonen and Luttinen, 2008, 2010; cf. Ito and Mahoney, 2006).

There are some indications that could link E-FP to a mantle plume. As mentioned before, the “plume–lithosphere” mixing curve of Ellam et al. (1992), reconstructed on the basis of Nd–Os isotope systematics of the Mwenzzi picrites, indicates that the loosely constrained Karoo “plume end-member” closely corresponds to the E-FP source component (Fig. 6). Moreover, the OIB-like source of E-FP has not been sampled by subsequently developed mid-ocean ridges (Figs. 4–5) thus questioning its presence in the upper convecting mantle. On the other hand, even if such upper mantle components existed, they would have likely been diluted by low-pressure high-degree peridotite partial melts typically formed in mid-ocean ridge settings (cf. Ito and Mahoney, 2006). Importantly, there is no geochemical evidence that would strictly associate E-FP with a mantle plume. For example, some of the alkaline volcanic rocks of the Maymecha–Kotuy region of the Siberian Traps CFB province that show very similar isotopic compositions to the E-FP (Figs. 4–6) have been linked to a major pyroxenitic component in the upper convecting mantle (Carlson et al., 2006). Furthermore, upper mantle has recently been estimated to contain approximately 5–10% of recycled (enriched) material on average (Cooper et al., 2009). Accordingly, it remains an open question whether the enriched component recorded by E-FP actually was introduced by a deep-seated mantle plume or formed an intrinsic part of the sublithospheric or lithospheric Gondwanan upper mantle (cf. Sections 6.1. and 6.2.2; Fig. 9).

In the case of the Vestfjella depleted types, the plume model is challenged by the geochemical evidence that supports their generation from Indian Ocean MORB-source upper mantle material. Why do these MORB-source magmas record the highest mantle potential

temperatures within the Karoo CFB province? Where are the derivatives of the highly magnesian melts that would be expected to form in the hottest parts of the plume itself? Potential answers to these questions are provided by the study on the Horingbai picrites (Paraná–Etendeka) that show evidence for komatiitic parental melts ($T_p \sim 1700$ °C) so dense that they were thought remain trapped at Moho depths (Thompson and Gibson, 2000). Unlike the dense plume-axis melts (cf. Thompson and Gibson, 2000), the hydrous, and thus relatively low-viscosity and low-density parental melts of the Vestfjella depleted types (derived from plume-entrained, hydrated upper mantle material) could have rapidly ascended through lithosphere without significant interaction with country rocks (cf. Arndt et al., 1998). The most straightforward explanation for the generation of the Vestfjella depleted types, however, is that they represent melts of hydrated MORB-source upper mantle that was internally heated beneath a supercontinent (Fig. 9b). In that case, such a process, accompanied by rifting and subsequent eruption of melts derived from heterogeneous subcontinental upper mantle, could also be held largely responsible for the generation of the Karoo CFBs (and possibly also contemporaneous Ferrar CFBs; cf. Fig. 1) (Fig. 9b; Coltice et al., 2007, 2009; cf. Silver et al., 2006). One possible weakness for this alternative is that the most recent models of the internal heating effect suggest maximum mantle potential temperatures of approximately ~ 1600 °C (Coltice et al., 2007) whereas temperatures of >1600 °C seem to have been required for the generation of the Vestfjella meimechites (Heinonen and Luttinen, 2010). We emphasize, however, that this marginal temperature difference is based on models that only take account limited number of variables and thus it should not be considered definitive.

In summary, our results provide strong support for the views of Coltice et al. (2009), although the slightly too high mantle potential temperatures (>1600 °C) calculated for D-FP are left unexplained by the current internal mantle heating model. Nevertheless, the SW Indian Ridge MORB-like chemical and isotope signature of the hottest parental magmas of the Karoo province (D-FP) are not obviously expected for the plume model and suggest that such a deep upwelling in the upper mantle is not required to explain the generation of the Karoo CFBs (cf. Jourdan et al., 2004, 2005, 2007a, 2007b, 2009; Coltice et al., 2009).

7. Conclusions

On the basis of Sr, Nd, Pb, and Os isotopic data on the Jurassic Karoo continental flood basalt-related highly magnesian dike rocks of

Vestfjella, western Dronning Maud Land (Antarctica), we present the following conclusions:

1. The previously recognized geochemical types (D-FP and E-FP) exhibit distinct isotopic signatures: (1) D-FP types are characterized by unradiogenic initial $^{87}\text{Sr}/^{86}\text{Sr}$ (0.7030–0.7036), radiogenic initial ϵ_{Nd} (from +4.8 to +8.3), and moderately unradiogenic initial $^{206}\text{Pb}/^{204}\text{Pb}$ (17.35–17.90), $^{207}\text{Pb}/^{204}\text{Pb}$ (15.42–15.49), $^{208}\text{Pb}/^{204}\text{Pb}$ (37.30–37.50), and $^{187}\text{Os}/^{188}\text{Os}$ (0.1256–0.1277) calculated at 180 Ma. (2) E-FP types are characterized by relatively more radiogenic initial $^{87}\text{Sr}/^{86}\text{Sr}$ (0.7043–0.7050), unradiogenic initial ϵ_{Nd} (from +1.8 to +3.6), similar initial $^{206}\text{Pb}/^{204}\text{Pb}$ (17.87–17.91), and more radiogenic initial $^{207}\text{Pb}/^{204}\text{Pb}$ (15.53–15.58), $^{208}\text{Pb}/^{204}\text{Pb}$ (37.76–37.82), and $^{187}\text{Os}/^{188}\text{Os}$ (0.1401–0.1425). Both types have avoided significant crustal contamination and crystallized from mantle-derived melts.
2. The isotopic characteristics of D-FP are indistinguishable from SW Indian Ridge MORBs and MORB-like dikes of Vestfjella and indicate long-term depleted, dominantly peridotitic sublithospheric upper mantle sources for this chemical type. Given the high temperatures required for the generation of ferropicrites and meimechites, we suggest that the D-FP magmas sampled hydrated and heated upper mantle material. The source of D-FP is likely to represent a depleted sublithospheric end-member for the dominantly SCLM-signatured Karoo lavas.
3. The isotopic characteristics of E-FP show general affinities to EM-signatured OIBs and ferropicrites from Paraná-Etendeka province and indicate pyroxene-rich mantle sources. Sr, Nd, and Pb isotopic modeling suggest that the source may have contained recycled oceanic crust with 5–20 vol.% of sediment material, but it may have also been generated by melt metasomatism in the upper mantle.
4. Given the strong affinity of D-FP and SW Indian Ridge MORBs, we speculate that heating of the upper mantle beneath the Gondwana supercontinent played an important role in Karoo CFB genesis. This would require higher mantle potential temperatures than predicted by the most recent internal heating models, however.

Supplementary materials related to this article can be found online at [doi:10.1016/j.chemgeo.2010.08.004](https://doi.org/10.1016/j.chemgeo.2010.08.004).

Acknowledgements

The comments of Fred Jourdan and an anonymous reviewer, and the editorial remarks by Bernard Bourdon helped to improve the manuscript and are highly appreciated. Nicolas Coltice provided additional comments on our presentation of the global mantle warming model. The FINNARP 2007 crew, especially Ilona Romu and Mika Kalakoski, are thanked for their assiduous support during the 2007–2008 field season at Vestfjella. Previous FINNARP expedition members (especially Henrik Grind, Mika Räisänen, and Saku Vuori) are also thanked for assisting in gathering samples for this study. Arto Peltola and Juhani Virkanen assisted with the sample preparations and Mary Horan and Timothy Mock assisted with the chemical separations and spectrometry at DTM, respectively. Hannu Huhma provided invaluable help with the isotope analyses at GSF. This work was supported by the Academy of Finland (grant nos. 210640 for J.H. and 129910 for A.L.), the Finnish Graduate School of Geology (for J.H.), and the Carnegie Institution of Washington, and is a contribution to IPY project Plates and Gates (#77; Eol 1264).

References

Adam, J., Green, T., 2006. Trace element partitioning between mica- and amphibole-bearing garnet lherzolite and hydrous basanitic melt: 1. Experimental results and the investigation of controls on partitioning behaviour. *Contributions to Mineralogy and Petrology* 152 (1), 1–17.

Anderson, D.L., 2007. The eclogite engine: chemical geodynamics as a Galileo thermometer. In: Foulger, G., Jurdy, D. (Eds.), *Plates, Plumes, and Planetary Processes: Geological Society of America Special Paper*, vol. 430, pp. 47–64.

Antonini, P., Piccirillo, E.M., Petrini, R., Civetta, L., D'Antonio, M., Orsi, G., 1999. Enriched mantle – Dupal signature in the genesis of the Jurassic Ferrar Tholeiites from Prince Albert Mountains (Victoria Land, Antarctica). *Contributions to Mineralogy and Petrology* 136 (1–2), 1–19.

Armstrong, R.A., Bristow, J.W., Cox, K.G., 1984. The Rooi Rand dyke swarm, southern Lebombo. In: Erlank, A.J. (Ed.), *Petrogenesis of the Volcanic Rocks of the Karoo Province. Geological Society of South Africa Special Publication* 13, 77–86.

Arndt, N.T., Lehnert, K., Vasil'ev, Y., 1995. Meimechites: highly magnesian lithosphere-contaminated alkaline magmas from deep subcontinental mantle. *Lithos* 34 (1–3), 41–59.

Arndt, N.T., Chauvel, C., Czamanske, G., Fedorenko, V., 1998. Two mantle sources, two plumbing systems: tholeiitic and alkaline magmatism of the Maymecha River basin, Siberian flood volcanic province. *Contributions to Mineralogy and Petrology* 133 (3), 297–313.

Barton Jr., J.M., Klemd, R., Allsopp, H.L., Auret, S.H., Copperthwaite, Y.E., 1987. The geology and geochronology of the Annandagstoppane granite, Western Dronning Maud Land, Antarctica. *Contributions to Mineralogy and Petrology* 97 (4), 488–496.

Bergman, S.C., 1987. Lamproites and other potassium-rich igneous rocks: a review of their occurrence, mineralogy and geochemistry. In: Fitton, J.G., Upton, B.G.J. (Eds.), *Alkaline Igneous Rocks. Geological Society of London Special Publication* 30, 103–190.

Betton, P.J., Armstrong, R.A., Manton, W.L., 1984. Variations in the lead isotopic composition of Karoo magmas. In: Erlank, A.J. (Ed.), *Petrogenesis of the volcanic rocks of the Karoo Province. Geological Society of South Africa Special Publication* 13, 331–339.

Bohrson, W.A., Spera, F.J., 2001. Energy-constrained open-system magmatic processes II: application of energy-constrained assimilation-fractional crystallization (EC-AFC) model to magmatic systems. *Journal of Petrology* 42 (5), 1019–1041.

Brewer, T.S., Rex, D., Guise, P.G., Hawkesworth, C.J., 1996. Geochronology of Mesozoic tholeiitic magmatism in Antarctica: implications for the development of the failed Weddell Sea rift system. In: Storey, B.C., King, E.C., Livermore, R.A. (Eds.), *Weddell Sea tectonics and Gondwana break-up. Geological Society Special Publications* 108, 45–61.

Carlson, R.W., 2005. Application of the Pt–Re–Os isotopic systems to mantle geochemistry and geochronology. *Lithos* 82 (3–4), 249–272.

Carlson, R.W., Nowell, G.M., 2001. Olivine-poor sources for mantle-derived magmas: Os and Hf isotopic evidence from potassic magmas of the Colorado Plateau. *Geochemistry, Geophysics, Geosystems* 2 (6). doi:10.1029/2000GC000128.

Carlson, R.W., Czamanske, G., Fedorenko, V., Ilupin, I., 2006. A comparison of Siberian meimechites and kimberlites: implications for the source of high-Mg alkalic magmas and flood basalts. *Geochemistry, Geophysics, Geosystems* 7 (11). doi:10.1029/2006GC001342.

Chesley, J.T., Righter, K., Ruiz, J., 2004. Large-scale mantle metasomatism: a Re/Os perspective. *Earth and Planetary Science Letters* 219 (1–2), 49–60.

Coltice, N., Phillips, B.R., Bertrand, H., Ricard, Y., Rey, P., 2007. Global warming of the mantle at the origin of flood basalts over supercontinents. *Geology* 35 (5), 391–394.

Coltice, N., Bertrand, H., Rey, P., Jourdan, F., Phillips, B.R., Ricard, Y., 2009. Global warming of the mantle beneath continents back to the Archaean. *Gondwana Research* 15 (3–4), 254–266.

Cooper, K.M., Eiler, J.M., Sims, K.W.W., Langmuir, C.H., 2009. Distribution of recycled crust within the upper mantle: Insights from the oxygen isotope composition of MORB from the Australian–Antarctic discordance. *Geochemistry, Geophysics, Geosystems* 10. doi:10.1029/2009GC002728.

Corner, B., 1994. Geological Evolution of western Dronning Maud Land within a Gondwana Framework: Geophysics Subprogramme. Final Project Report to SACAR. Department of Geophysics, Witwatersrand University, South Africa (21 pp.).

Cox, K.G., 1988. The Karoo province. In: MacDougall, J.D. (Ed.), *Continental Flood Basalts. Kluwer Academic Publishers, Dordrecht*, pp. 239–271.

Cox, K.G., Bristow, J.W., 1984. The Sabie River Basalt Formation of the Lebombo monocline and south-east Zimbabwe. In: Erlank, A.J. (Ed.), *Petrogenesis of the Volcanic Rocks of the Karoo Province. Geological Society of South Africa Special Publication* 13, 125–147.

Curtis, M.L., Riley, T.R., Owens, W.H., Leat, P.T., Duncan, R.A., 2008. The form, distribution and anisotropy of magnetic susceptibility of Jurassic dykes. In H.U. Sverdrupfjella, Dronning Maud Land, Antarctica. Implications for Dyke Swarm Emplacement. *Journal of Structural Geology* 30 (11), 1429–1447.

Dale, C.W., Pearson, D.G., Starkey, N.A., Stuart, F.M., Ellum, R.M., Larsen, L.M., Fitton, J.G., Macpherson, C.G., 2009. Osmium isotopes in Baffin Island and West Greenland picrites: implications for the $^{187}\text{Os}/^{188}\text{Os}$ composition of the convecting mantle and the nature of high $^3\text{He}/^4\text{He}$ mantle. *Earth and Planetary Science Letters* 278 (3–4), 267–277.

DePaolo, D.J., 1981. Trace element and isotopic effects of combined wallrock assimilation and fractional crystallization. *Earth and Planetary Science Letters* 53 (2), 189–202.

Duncan, A.R., Armstrong, R.A., Erlank, A.J., Marsh, J.S., Watkins, R.T., 1990. MORB-related dolerites associated with the final phases of Karoo flood basalt volcanism in Southern Africa. In: Parker, A.J., Rickwood, P.C., Tucker, D.H. (Eds.), *Mafic Dykes and Emplacement Mechanisms. Proceedings of the International Dyke Conference 2, Balkema, Rotterdam*, pp. 119–129.

Duncan, R.A., Hooper, P.R., Rehacek, J., Marsh, J.S., Duncan, A.R., 1997. The timing and duration of the Karoo igneous event, southern Gondwana. *Journal of Geophysical Research* 102 (B8), 18,127–18,138.

Eisele, J., Sharma, M., Galer, S.J.G., Blichert-Toft, J., Devey, C.W., Hofmann, A.W., 2002. The role of sediment recycling in EM-1 inferred from Os, Pb, Hf, Nd, Sr isotope and

- trace element systematics of the Pitcairn Hotspot. *Earth and Planetary Science Letters* 196 (3–4), 197–212.
- Elburg, M., Goldberg, A., 2000. Age and geochemistry of Karoo dolerite dykes from Northeast Botswana. *Journal of African Earth Sciences* 31 (3–4), 539–554.
- Elkins-Tanton, L.T., 2005. Continental magmatism caused by lithospheric delamination. In: Foulger, G., Natland, J.H., Prensall, D.C., Anderson, D.L. (Eds.), *Plates, Plumes, and Paradigms: Geological Society of America Special Paper*, vol. 388, pp. 449–461.
- Elkins-Tanton, L.T., Draper, D.S., Agee, C.B., Jewell, J., Thorpe, A., Hess, P.C., 2007. The last lavas erupted during the main phase of the Siberian flood volcanic province: results from experimental petrology. *Contributions to Mineralogy and Petrology* 153 (2), 191–209.
- Ellam, R.M., 2006. New constraints on the petrogenesis of the Nuanetsi picrite basalts from Pb and Hf isotope data. *Earth and Planetary Science Letters* 245 (1–2), 153–161.
- Ellam, R.M., Cox, K.G., 1989. A proterozoic lithospheric source for Karoo magmatism: evidence from the Nuanetsi picrites. *Earth and Planetary Science Letters* 92 (2), 207–218.
- Ellam, R.M., Cox, K.G., 1991. An interpretation of Karoo picrite basalts in terms of interaction between asthenospheric magmas and the mantle lithosphere. *Earth and Planetary Science Letters* 105 (1–3), 330–342.
- Ellam, R.M., Carlson, R.W., Shirey, S.B., 1992. Evidence from Re–Os isotopes for plume–lithosphere mixing in Karoo flood basalt genesis. *Nature* 359 (6397), 718–721.
- Esser, B.K., Turekian, K.K., 1993. The osmium isotopic composition of the continental crust. *Geochimica et Cosmochimica Acta* 57 (13), 3093–3104.
- Faure, G., Bowman, J.R., Elliot, D.H., Jones, L.M., 1974. Strontium isotope composition and petrogenesis of the Kirkpatrick basalt, Queen Alexandra Range, Antarctica. *Contributions to Mineralogy and Petrology* 3 (3), 153–169.
- Florentini, M.L., Beresford, S.W., Delouie, E., Hanski, E.J., Stone, W.E., Pearson, N.J., 2008. The role of mantle-derived volatiles in the petrogenesis of Palaeoproterozoic ferropicrites in the Pechenga greenstone belt, northwestern Russia: insights from in-situ microbeam and nanobeam analysis of hydromagmatic amphibole. *Earth and Planetary Science Letters* 268 (1–2), 2–14.
- Fitton, J.G., Saunders, A.D., Norry, M.J., Hardarson, B.S., Taylor, R.N., 1997. Thermal and chemical structure of the Iceland plume. *Earth and Planetary Science Letters* 153 (3–4), 197–208.
- Fitton, J.G., Saunders, A.D., Kempton, P.D., Hardarson, B.S., 2003. Does depleted mantle form an intrinsic part of the Iceland plume? *Geochimica et Cosmochimica Acta* 67 (3), 1029–1034. doi:10.1029/2002GC000424.
- Foulger, G.R., 2007. The “plate” model for the genesis of melting anomalies. In: Foulger, G., Jurdy, D. (Eds.), *Plates, Plumes, and Planetary Processes: Geological Society of America Special Paper*, vol. 430, pp. 1–28.
- Furnes, H., Vad, E., Austrheim, H., Mitchell, J.G., Garmann, L.F., 1987. Geochemistry of basalt lavas from Vestfjella and adjacent areas, Dronning Maud Land, Antarctica. *Lithos* 20 (5), 337–356.
- Gibson, S.A., Thompson, R.N., Dickin, A.P., 2000. Ferropicrites: geochemical evidence for Fe-rich streaks in upwelling mantle plumes. *Earth and Planetary Science Letters* 174 (3–4), 355–374.
- Groenewald, P.B., Moyes, A.B., Grantham, G.H., Krynanuw, J.R., 1995. East Antarctic crustal evolution: geological constraints and modelling in western Dronning Maud Land. *Precambrian Research* 75 (3–4), 231–250.
- Gurnis, M., 1988. Large-scale mantle convection and the aggregation and dispersal of supercontinents. *Nature* 332 (6166), 695–699.
- Hargraves, R.B., Rehacek, J., Hooper, P.R., 1997. Palaeomagnetism of the Karoo igneous rocks in Southern Africa. *South African Journal of Geology* 100 (3), 195–212.
- Harmer, R.E., Lee, C.A., Eglington, B.M., 1998. A deep mantle source for carbonatite magmatism: evidence from the nephelinites and carbonatites of the Buhera District, SE Zimbabwe. *Earth and Planetary Science Letters* 158 (3–4), 131–142.
- Harris, C., Marsh, J.S., Duncan, A.R., Erlank, A.J., 1990. The petrogenesis of the Kirwan Basalts of Dronning Maud Land, Antarctica. *Journal of Petrology* 31 (2), 341–369.
- Harris, C., Watters, B.R., Groenewald, P.B., 1991. Geochemistry of the Mesozoic regional basic dykes of western Dronning Maud Land, Antarctica. *Contributions to Mineralogy and Petrology* 107 (1), 100–111.
- Hart, S.R., 1988. Heterogeneous mantle domains: signatures, genesis and mixing chronologies. *Earth and Planetary Science Letters* 90 (3), 273–296.
- Hauri, E.H., Hart, S.R., 1993. Re–Os isotope systematics of HIMU and EMII oceanic island basalts from the South Pacific Ocean. *Earth and Planetary Science Letters* 114 (2–3), 353–371.
- Hauri, E.H., Gaetani, G.A., Green, T.H., 2006. Partitioning of water during melting of the Earth's upper mantle at H₂O-undersaturated conditions. *Earth and Planetary Science Letters* 248 (3–4), 715–734.
- Hawkesworth, C.J., Marsh, J.S., Duncan, A.R., Erlank, A.J., Norry, M.J., 1984. The role of continental lithosphere in the generation of the Karoo volcanic rocks: evidence from combined Nd- and Sr-isotope studies. In: Erlank, A.J. (Ed.), *Petrogenesis of the Volcanic Rocks of the Karoo Province. Geological Society of South Africa Special Publication* 13, 341–354.
- Heinonen, J.S., Luttinen, A.V., 2008. Jurassic dikes of Vestfjella, western Dronning Maud Land, Antarctica: geochemical tracing of ferropicrite sources. *Lithos* 105 (3–4), 347–364.
- Heinonen, J.S., Luttinen, A.V., 2010. Mineral chemical evidence for extremely magnesian subalkaline melts from the Antarctic extension of the Karoo large igneous province. *Mineralogy and Petrology* 99, 201–217.
- Hergt, J.M., Peate, D.W., Hawkesworth, C.J., 1991. The petrogenesis of Mesozoic Gondwana low-Ti flood basalts. *Earth and Planetary Science Letters* 105 (1–3), 134–148.
- Herzberg, C., O'Hara, M.J., 2002. Plume-associated ultramafic magmas of Phanerozoic age. *Journal of Petrology* 43 (10), 1857–1883.
- Hoefs, J., Faure, G., Elliot, D.H., 1980. Correlation of $\delta^{18}\text{O}$ and initial $^{87}\text{Sr}/^{86}\text{Sr}$ ratios in Kirkpatrick Basalt on Mt. Falla, Transantarctic Mountains. *Contributions to Mineralogy and Petrology* 75, 199–203.
- Horan, M.F., Walker, R.J., Fedorenko, V.A., Czamanske, G.K., 1995. Osmium and neodymium isotopic constraints on the temporal and spatial evolution of Siberian flood basalt sources. *Geochimica et Cosmochimica Acta* 59 (24), 5159–5168.
- Ito, G., Mahoney, J.J., 2006. Melting a high $^3\text{He}/^4\text{He}$ source in a heterogeneous mantle. *Geochimica et Cosmochimica Acta* 70 (5). doi:10.1029/2005GC001158.
- Jackson, M.G., Dasgupta, R., 2008. Compositions of HIMU, EM1, and EM2 from global trends between radiogenic isotopes and major elements in ocean island basalts. *Earth and Planetary Science Letters* 276 (1–2), 175–186.
- Jackson, M.G., Hart, S.R., Saal, A.E., Shimizu, N., Kurz, M.D., Blusztajn, J.S., Skovgaard, A.C., 2008. Globally elevated titanium, tantalum, and niobium (TITAN) in ocean island basalts with high $^3\text{He}/^4\text{He}$. *Geochimica et Cosmochimica Acta* 72 (4). doi:10.1029/2007GC001876.
- Jacobs, J., Thomas, R.J., Weber, K., 1993. Accretion and indentation tectonics at the southern edge of the Kaapvaal Craton during the Kibaran (Grenville) Orogeny. *Geology* 21 (3), 203–206.
- Jacobs, J., Fanning, C.M., Henjes-Kunst, F., Olesch, M., Paech, H., 1998. Continuation of the Mozambique Belt into East Antarctica: Grenville-age metamorphism and polyphase Pan-African high-grade events in central Dronning Maud Land. *Journal of Geology* 106 (4), 385–406.
- Jacobs, J., Bauer, W., Fanning, C.M., 2003a. Late Neoproterozoic/early Palaeozoic events in central Dronning Maud Land and significance for the southern extension of the East African Orogen into East Antarctica. *Precambrian Research* 126 (1–2), 27–53.
- Jacobs, J., Fanning, C.M., Bauer, W., 2003b. Timing of Grenville-age vs. Pan-African medium- to high grade metamorphism in western Dronning Maud Land (East Antarctica) and significance for correlations in Rodinia and Gondwana. *Precambrian Research* 125 (1–2), 1–20.
- Janney, P.E., le Roex, A.P., Carlson, R.W., 2005. Hafnium isotope and trace element constraints on the nature of mantle heterogeneity beneath the central Southwest Indian Ridge (13°E to 47°E). *Journal of Petrology* 46 (12), 2427–2464.
- Johnson, K.T.M., 1998. Experimental determination of partition coefficients for rare earth and high-field-strength elements between clinopyroxene, garnet, and basaltic melt at high pressure. *Contributions to Mineralogy and Petrology* 133 (1–2), 60–68.
- Johnson, D.M., Hooper, P.R., Conrey, R.M., 1999. XRF analysis of rocks and minerals for major and trace elements on a single low dilution Li-tetraborate fused bead. *Advances in X-Ray Analysis* 41, 843–867.
- Jourdan, F., Feraud, G., Bertrand, H., Kampunzu, A.B., Tshoso, G., Le Gall, B., Tiercelin, J.J., Capiez, P., 2004. The Karoo triple junction questioned: evidence from Jurassic and Proterozoic $^{40}\text{Ar}/^{39}\text{Ar}$ ages and geochemistry of the giant Okavango dike swarm (Botswana). *Earth and Planetary Science Letters* 222 (3–4), 989–1006.
- Jourdan, F., Feraud, G., Bertrand, H., Kampunzu, A.B., Tshoso, G., Watkeys, M.K., Le Gall, B., 2005. Karoo large igneous province: Brevity, origin, and relation to mass extinction questioned by new $^{40}\text{Ar}/^{39}\text{Ar}$ age data. *Geology* 33 (9), 745–748.
- Jourdan, F., Feraud, G., Bertrand, H., Watkeys, M.K., Kampunzu, A.B., Le Gall, B., 2006. Basemant control on dyke distribution in large igneous provinces: case study of the Karoo triple junction. *Earth and Planetary Science Letters* 241 (1–2), 307–322.
- Jourdan, F., Bertrand, H., Schaerer, U., Blichert-Toft, J., Feraud, G., Kampunzu, A.B., 2007a. Major and trace element and Sr, Nd, Hf, and Pb isotope compositions of the Karoo large igneous province, Botswana–Zimbabwe: lithosphere vs mantle plume contribution. *Journal of Petrology* 48 (6), 1043–1077.
- Jourdan, F., Feraud, G., Bertrand, H., Watkeys, M.K., 2007b. From flood basalts to the inception of oceanization: example from the $^{40}\text{Ar}/^{39}\text{Ar}$ high-resolution picture of the Karoo large igneous province. *Geochimica et Cosmochimica Acta* 71 (2). doi:10.1029/2006GC001392.
- Jourdan, F., Bertrand, H., Feraud, G., Le Gall, B., Watkeys, M.K., 2009. Lithospheric mantle evolution monitored by overlapping large igneous provinces: case study in southern Africa. *Lithos* 107 (3–4), 257–268.
- Jukes, L.M., 1972. The geology of north-eastern Heimefrontfjella, Dronning Maud Land. *British Antarctic Survey Scientific Reports* 65 (44 pp.).
- Kelley, K.A., Plank, T., Farr, L., Ludden, J., Staudigel, H., 2005. Subduction cycling of U, Th, and Pb. *Earth and Planetary Science Letters* 234 (3–4), 369–383.
- Keppler, H., 1996. Constraints from partitioning experiments on the composition of subduction-zone fluids. *Nature* 380 (6571), 237–240.
- Kerr, A.C., Saunders, A.D., Tarney, J., Berry, N.H., Hards, V.L., 1995. Depleted mantle–plume geochemical signatures: no paradox for plume theories. *Geology* 23 (9), 843–846.
- Klein, E.M., 2003. Geochemistry of the igneous ocean crust. In: Rudnick, R.L. (Ed.), *The Crust, Treatise on Geochemistry* 3. Elsevier-Pergamon, Oxford, pp. 433–463.
- Knaack, C., Cornelius, S.B., Hooper, P.R., 1994. Trace element analyses of rocks and minerals by ICP-MS. *GeoAnalytical Lab*, Washington State University, <http://www.sees.wsu.edu/Geolab/equipment/icpms.html>.
- Kogiso, T., Tatsumi, Y., Nakano, S., 1997. Trace element transport during dehydration processes in the subducted oceanic crust: 1. Experiments and implications for the origin of ocean island basalts. *Earth and Planetary Science Letters* 148 (1–2), 193–205.
- Kreissig, K., Naegler, T.F., Kramers, J.D., van Reenen, D.D., Smit, C.A., 2000. An isotopic and geochemical study of the northern Kaapvaal Craton and the Southern Marginal Zone of the Limpopo Belt: are they juxtaposed terranes? *Lithos* 50 (1–3), 1–25.
- Krynanuw, J.R., Hunter, D.R., Wilson, A.H., 1988. Emplacement of sills into wet sediments at Grunehogna, western Dronning Maud Land, Antarctica. *Journal of the Geological Society of London* 145, 1019–1032.
- Krynanuw, J.R., Watters, B.R., Hunter, D.R., Wilson, A.H., 1991. A review of the field relations, petrology and geochemistry of the Borgmassivet intrusions in the Grunehogna Province, western Dronning Maud Land, Antarctica. In: Thomsson, M.R.A., Crame, J.A., Thomsson, J.W. (Eds.), *Geological Evolution of Antarctica, Proceedings of the Fifth International Symposium on Antarctic Earth Sciences*. Cambridge University Press, Cambridge, pp. 33–39.

- le Roex, A.P., Dick, H.J.B., Fisher, R.L., 1989. Petrology and geochemistry of MORB from 25°E to 46°E along the Southwest Indian Ridge: evidence for contrasting styles of mantle enrichment. *Journal of Petrology* 30 (4), 947–986.
- Leat, P.T., Luttinen, A.V., Storey, B.C., Millar, I.L., 2006. Sills of the Theron Mountains, Antarctica: evidence for long distance transport of mafic magmas during Gondwana break-up. In: Hanski, E.J., Mertanen, S., Rämö, O.T., Vuollo, J. (Eds.), *Dyke Swarms: Time Markers of Crustal Evolution*. Taylor & Francis, Abingdon, pp. 183–199.
- Lee, C.A., Yin, Q., Rudnick, R.L., Chesley, J.T., Jacobsen, S.B., 2000. Osmium isotopic evidence for Mesozoic removal of lithospheric mantle beneath the Sierra Nevada, California. *Science* 289 (5486), 1912–1916.
- Luttinen, A.V., Furnes, H., 2000. Flood basalts of Vestfjella: Jurassic magmatism across an Archaean–Proterozoic lithospheric boundary in Dronning Maud Land, Antarctica. *Journal of Petrology* 41 (8), 1271–1305.
- Luttinen, A.V., Siivola, J.U., 1997. Geochemical characteristics of Mesozoic lavas and dikes from Vestfjella, Dronning Maud Land: recognition of three distinct chemical types. In: Ricci, C.A. (Ed.), *The Antarctic Region: Geological Evolution and Processes*. Siena: Terra Antarctica Publications, Italy, pp. 495–503.
- Luttinen, A.V., Rämö, O.T., Huhma, H., 1998. Neodymium and strontium isotopic and trace element composition of a Mesozoic CFB suite from Dronning Maud Land, Antarctica: implications for lithosphere and asthenosphere contributions to Karoo magmatism. *Geochimica et Cosmochimica Acta* 62 (15), 2701–2714.
- Luttinen, A.V., Zhang, X., Folland, K.A., 2002. 159 Ma Kfajakebeinet lamproites (Dronning Maud Land, Antarctic) and their implications for Gondwana breakup processes. *Geological Magazine* 139 (5), 525–539.
- Mahoney, J., le Roex, A.P., Peng, Z., Fisher, R.L., Natland, J.H., 1992. Southwestern limits of Indian Ocean ridge mantle and the origin of low ²⁰⁶Pb/²⁰⁴Pb mid-ocean ridge basalt: isotope systematics of the central Southwest Indian Ridge (17°–50°E). *Journal of Geophysical Research* 97 (B13), 19,771–19,790.
- McDonough, W.F., Frey, F.A., 1989. Rare earth elements in upper mantle rocks. In: Lipin, B.R., McKay, G.A. (Eds.), *Geochemistry and Mineralogy of Rare Earth Elements: Reviews in Mineralogy* 21, Mineralogical Society of America, pp. 100–145.
- Morgan, W.J., 1971. Convection plumes in the lower mantle. *Nature* 230 (5288), 42–43.
- Moyes, A.B., Krynanaw, J.R., Barton Jr., J.M., 1995. The age of the Ritscherflya Supergroup and Borgmassivet Intrusions, Dronning Maud Land, Antarctica. *Antarctic Science* 7 (1), 87–97.
- Nishio, Y., Nakai, S., Ishii, T., Sano, Y., 2007. Isotope systematics of Li, Sr, Nd, and volatiles in Indian Ocean MORBs of the Rodrigues triple junction: constraints on the origin of the DUPAL anomaly. *Geochimica et Cosmochimica Acta* 71 (3), 745–759.
- Niu, Y., O'Hara, M.J., 2003. Origin of ocean island basalts: a new perspective from petrology, geochemistry, and mineral physics considerations. *Journal of Geophysical Research* 108 (B4). doi:10.1029/2002JB002048.
- Olive, V., Ellam, R.M., Harte, B., 1997. A Re–Os isotope study of ultramafic xenoliths from the Matsoku kimberlite. *Earth and Planetary Science Letters* 150 (1–2), 129–140.
- Peters, M., Haverkamp, B., Emmermann, R., Kohnen, H., Weber, K., 1991. Palaeomagnetism, K–Ar dating and geodynamic setting of igneous rocks in western and central Neuschwabenland, Antarctica. In: Thomson, M.R.A., Crame, J.A., Thomson, J.W. (Eds.), *Geological Evolution of Antarctica, Proceedings of the Fifth International Symposium on Antarctic Earth Sciences*. Cambridge University Press, Cambridge, pp. 549–555.
- Plank, T., Langmuir, C., 1998. The chemical composition of subducting sediment and its consequences for the crust and mantle. *Chemical Geology* 145 (3–4), 325–394.
- Putirka, K.D., 2008. Excess temperatures at ocean islands: implications for mantle layering and convection. *Geology* 36 (4), 283–286.
- Rämö, O.T., 1991. Petrogenesis of the Proterozoic rapakivi granites and related basic rocks of southeastern Fennoscandia: Nd and Pb isotopic and general geochemical constraints. *Geological Survey of Finland Bulletin* 355 (161 pp.).
- Rämö, O.T., Luttinen, A.V., Andersen, T., Kurhila, M.I., 2008. Mesoproterozoic A-type granites in Mannefalknausane, western Dronning Maud Land, Antarctica: U–Pb (LAMMS) zircon chronology and Nd (whole-rock ID-TIMS) and Hf (zircon LAMS) isotope geochemistry. In: Ojala, A. (Ed.), *Program and Abstracts, Congress of the International Polar Year 2007/08*, Geological Survey of Finland, p. 45.
- Rehkämper, M., Hofmann, A., 1997. Recycled ocean crust and sediment in Indian Ocean MORB. *Earth and Planetary Science Letters* 147 (1–4), 93–106.
- Reisberg, L., Zindler, A., Marcantonio, F., White, W.M., Wyman, D., Weaver, B., 1993. Os isotope systematics in ocean island basalts. *Earth and Planetary Science Letters* 120 (3–4), 149–167.
- Richards, M.A., Griffiths, R.W., 1989. Thermal entrainment by deflected mantle plumes. *Nature* 342 (6252), 900–902.
- Richards, M.A., Duncan, R.A., Courtillot, V.E., 1989. Flood basalts and hot-spot tracks: plume heads and tails. *Science* 246 (4926), 103–107.
- Riley, T.R., Leat, P.T., Curtis, M.L., Millar, I.L., Duncan, R.A., Fazel, A., 2005. Early–Middle Jurassic dolerite dykes from Western Dronning Maud Land (Antarctica): identifying mantle sources in the Karoo Large Igneous Province. *Journal of Petrology* 46 (7), 1489–1524.
- Roy-Barman, M., Allègre, C.J., 1994. ¹⁸⁷Os/¹⁸⁶Os ratios of mid-ocean ridge basalts and abyssal peridotites. *Geochimica et Cosmochimica Acta* 58 (22), 5043–5054.
- Rudnick, R.L., Gao, S., 2003. The composition of the continental crust. In: Rudnick, R.L. (Ed.), *The Crust, Treatise on Geochemistry* 3. Elsevier-Perigamon, Oxford, pp. 1–64.
- Saal, A.E., Rudnick, R.L., Ravizza, G.E., Hart, S.R., 1998. Re–Os isotope evidence for the composition, formation and age of the lower continental crust. *Nature* 393 (6680), 58–61.
- Salteras, V.J.M., Stracke, A., 2004. Composition of the depleted mantle. *Geochemistry, Geophysics, Geosystems* 5 (5). doi:10.1029/2003GC000597.
- Saunders, A.D., Storey, M., Kent, R.W., Norry, M.J., 1992. Consequences of plume–lithosphere interactions. In: Storey, B.C., Alabaster, T., Pankhurst, R.J. (Eds.), *Magmatism and the Causes of Continental Break-up*. Geological Society Special Publications 68, 41–60.
- Segev, A., 2002. Flood basalts, continental breakup and the dispersal of Gondwana: evidence for periodic migration of upwelling mantle flows (plumes). *European Geosciences Union Stephan Mueller Special Publication Series* 2, 171–191.
- Shirey, S.B., Walker, R.J., 1998. The Re–Os isotope system in cosmochemistry and high-temperature geochemistry. *Annual Review of Earth and Planetary Sciences* 26, 423–500.
- Silver, P.G., Behn, M.D., Kelley, K.A., Schmitz, M., Savage, B., 2006. Understanding cratonic flood basalts. *Earth and Planetary Science Letters* 245 (1–2), 190–201.
- Simon, N.S., Carlson, R.W., Graham Pearson, D., Davies, G.R., 2007. The origin and evolution of the Kaapvaal cratonic lithospheric mantle. *Journal of Petrology* 48 (3), 589–625.
- Smith, C.B., 1983. Pb, Sr and Nd isotopic evidence for sources of southern African Cretaceous kimberlites. *Nature* 304 (5921), 51–54.
- Sobolev, A.V., Hofmann, A.W., Brüggemann, G., Batanova, V.G., Kuzmin, D.V., 2008. A quantitative link between recycling and osmium isotopes. *Science* 321 (5888), 536.
- Spera, F.J., Bohrsen, W.A., 2001. Energy-constrained open-system magmatic processes I: general model and energy-constrained assimilation and fractional crystallization (EC-AFC) formulation. *Journal of Petrology* 42 (5), 999–1018.
- Storey, B.C., Alabaster, T., Hole, M.J., Pankhurst, R.J., Wever, H.E., 1992. Role of subduction-plate boundary forces during the initial stages of Gondwana break-up: evidence from the proto-Pacific margin of Antarctica. In: Storey, B.C., Alabaster, T., Pankhurst, R.J. (Eds.), *Magmatism and the Causes of Continental Break-up*. Geological Society Special Publications 68, 149–163.
- Stracke, A., Bizimis, M., Salteras, V.J.M., 2003. Recycling oceanic crust: quantitative constraints. *Geochemistry, Geophysics, Geosystems* 4 (3). doi:10.1029/2001GC000223.
- Sun, S.S., McDonough, W.F., 1989. Chemical and isotopic systematics of oceanic basalts: implications for mantle composition and processes. In: Saunders, A.D., Norry, M.J. (Eds.), *Magmatism in the Ocean Basins*. Geological Society Special Publications 42, 313–345.
- Sweeney, R.J., Falloon, T.J., Green, D.H., Tatsumi, Y., 1991. The mantle origins of Karoo picrites. *Earth and Planetary Science Letters* 107 (2), 256–271.
- Sweeney, R.J., Duncan, A.R., Erlank, A.J., 1994. Geochemistry and petrogenesis of central Lebombo basalts of the Karoo igneous province. *Journal of Petrology* 35 (1), 95–125.
- Talarico, F., Borsi, L., Lombardo, B., 1995. Relict granulites in the Ross Orogen of northern Victoria Land (Antarctica) II. Geochemistry and palaeo-tectonic implications. *Precambrian Research* 75 (3–4), 157–174.
- Thompson, R.N., Gibson, S.A., 2000. Transient high temperatures in mantle plume heads inferred from magnesium olivines in Phanerozoic picrites. *Nature* 407 (6803), 502–506.
- Thompson, R.N., Gibson, S.A., Dickin, A.P., Smith, P.M., 2001. Early Cretaceous basalt and picrite dykes of the southern Etendeka region, NW Namibia: windows into the role of the Tristan mantle plume in Parana-Etendeka magmatism. *Journal of Petrology* 42 (11), 2049–2081.
- Todd, W., Cliff, R.A., Hanser, A., Hofmann, A.W., 1996. Evaluation of a ²⁰²Pb–²⁰⁵Pb double spike for high-precision lead isotope analysis. In: Basu, A.R., Hart, S.R. (Eds.), *Earth Processes: Reading the Isotopic Code: Geophysical Monograph*, 95, pp. 429–437.
- Tuff, J., Takahashi, E., Gibson, S.A., 2005. Experimental constraints on the role of garnet pyroxenite in the genesis of high-Fe mantle plume derived melts. *Journal of Petrology* 46 (10), 2023–2058.
- Vuori, S.K., Luttinen, A.V., 2003. The Jurassic gabbroic intrusion of Utpostane and Muren: insights into Karoo-related plutonism in Dronning Maud Land, Antarctica. *Antarctic Science* 15 (2), 283–301.
- Walker, R.J., Shirey, S.B., Carlson, R.W., Morgan, J.W., 1989. Os, Sr, Nd, and Pb isotope systematics of Southern African peridotite xenoliths: implications for the chemical evolution of subcontinental mantle. *Geochimica et Cosmochimica Acta* 53 (7), 1583–1595.
- Wang, Q., Wyman, D.A., Xu, J., Wan, Y., Li, C., Zi, F., Jiang, Z., Qiu, H., Chu, Z., Zhao, Z., Dong, Y., 2008. Triassic Nb-enriched basalts, magnesian andesites, and adakites of the Qiangtang Terrane (central Tibet): evidence for metasomatism by slab-derived melts in the mantle wedge. *Contributions to Mineralogy and Petrology* 155 (4), 473–490.
- White, W.M., Hofmann, A.W., 1982. Sr and Nd isotope geochemistry of oceanic basalts and mantle evolution. *Nature* 296 (5860), 821–825.
- Wilson, A.H., Shirey, S.B., Carlson, R.W., 2003. Archaean ultra-depleted komatiites formed by hydrous melting of cratonic mantle. *Nature* 423 (6942), 858–861.
- Wolmarans, L.C., Kent, K.E., 1982. Geological investigations in western Dronning Maud Land, Antarctica – a synthesis. *South African Journal of Antarctic Research (Supplements)* 2 (93 pp.).
- Woodhead, J.D., Devey, C.W., 1993. Geochemistry of the Pitcairn seamounts I: source character and temporal trends. *Earth and Planetary Science Letters* 116 (1–4), 81–99.
- Workman, R.K., Hart, S.R., 2005. Major and trace element composition of the depleted MORB mantle (DMM). *Earth and Planetary Science Letters* 231 (1–2), 53–72.
- Workman, R.K., Hart, S.R., Jackson, M., Regelous, M., Farley, K.A., Blusztajn, J., Kurz, M., Staudigel, H., 2004. Recycled metasomatized lithosphere as the origin of the enriched mantle II (EM2) end-member: evidence from the Samoan volcanic chain. *Geochemistry, Geophysics, Geosystems* 5. doi:10.1029/2003GC000623.
- Zhang, X., Luttinen, A.V., Elliot, D.H., Larsson, K., Folland, K.A., 2003. Early stages of Gondwana breakup: the ⁴⁰Ar/³⁹Ar geochronology of Jurassic basaltic rocks from western Dronning Maud Land, Antarctica, and implications for the timing of magmatic and hydrothermal events. *Journal of Geophysical Research* 108 (B9), 2449. doi:10.1029/2001JB001070.
- Zindler, A., Hart, S.R., 1986. Chemical geodynamics. *Annual Review of Earth and Planetary Sciences* 14, 493–571.